0

Contents

1 Introduction

1.1 Measuring the Angles of the Unitarity Triangle in B Decays

The Standard Model of particle interactions makes explicit predictions for CP violation that can be tested extensively using neutral B mesons. Here we address the processes $B^0 \to \rho\pi$, which will be an important part of these tests, as emphasized by Aleksan et al. [1], Lipkin et al. [2] and by Snyder and Quinn [3]. Some recent studies of $B \to \rho\pi$ have been directed towards the BaBar detector at SLAC's PEP-II facility [4, 5].

The neutral B meson system provides the opportunity to measure quantities directly related to the unitarity triangle, *whose angles are α, β, and γ*, without uncertainties due to strong interaction effects. This is particularly true for the decay $B^0 \to J/\psi K_S$ (we generally include the CP conjugate process without explicitly displaying it). These decays proceed primarily through $b \to c\bar{c}s$. Because these decays involve do not involve transitions between the first and third generations, no complex CKM matrix elements appear. CP violation is introduced only through the oscillations between B^0 and $\overline{B}^0$. The Standard Model predicts that oscillations introduce a phase 2β *between decays that occur directly from B^0 and those that occur from $\overline{B}^0$ via mixing.*

Another contribution to $B \to J/\psi K_S$, the so-called penguin, comes from a higher order effect dominated by $\overline{b} \to W^+\overline{t}$, $W^+\overline{t} \to \overline{s}g$, where g is a gluon that turns into $c\overline{c}$. The weak interactions here involve only the second and third generations, as well. The same analysis applies to the penguin contribution where t is replaced by c. Thus the conclusion based on the tree diagram is unchanged: $B \to J/\psi K_S$ measures the phase introduced by mixing, which in the Standard Model is 2β.

The decay $B^0 \to \pi\pi$ is attractive because the final state is an eigenstate of CP, just as in $B^0 \to J/\psi K_S$. The underlying quark process is dominantly $b \to u\overline{u}d$. This does involve a first-to-third generation transition and introduces the angle γ. As shown below, if mixing is given by the Standard Model, it is always the combination $\gamma + \beta$ that occurs. If it is assumed that the unitarity triangle is indeed a triangle, we have $\alpha + \beta + \gamma = \pi$, so measuring $\gamma + \beta$ is equivalent to measuring α. For this reason $B^0 \to \pi\pi$ is generally viewed as a means of measuring α.

There is a penguin contribution to $B^0 \to \pi\pi$, again dominated by the $\overline{t}$ intermediate: $\overline{b} \to W^+\overline{t}$, $W^+\overline{t} \to \overline{d}g$. This introduces another complex CKM matrix element so it is no longer true that only the combination $\gamma+\beta$ occurs. This makes the extraction of α much more difficult than that of β. To disentangle the penguin from the basic (tree) amplitude, we note that the penguin process can change isospin by at most $1/2$ as only the *transition from $\overline{b}$ to $\overline{d}$ contributes.* The tree contribution, $b \to u\overline{u}d$, can change isospin by $3/2$. It follows that the $\Delta I = 3/2$ process is free from penguin effects. This imposes a heavy burden: all the contributing amplitudes, tree and penguin, including their phases, must be determined from the data in order to isolate the $\Delta I = 3/2$ piece.

1.2 Measuring α in $B \to \rho\pi$

The full determination of α is possible from measurements of the time-dependent decays to $\pi^+\pi^-$, together with total rates to $\pi^\pm\pi^0$ and $\pi^0\pi^0$ [6, 7]. Unfortunately, the rates for these processes are small: CLEO has reported a branching ratio for $B^0 \to \pi^+\pi^-$ of $0.47^{+0.18}_{-0.15} \pm 0.13 \times 10^{-5}$ [8] . Moreover, there are reasons to expect the $\pi^0\pi^0$ final state to be even less frequent. The measurement of α in $B^0 \to \pi\pi$ will require quite a long time at the PEP-II and KEK asymmetric

e^+e^- colliders at their design luminosities. The higher event rates in hadron machines will be an advantage, but the π^0's present particular problems in this environment and K/π separation is essential. The larger branching ratio for $B^0 \to K^+\pi^-$, $18.8\ ^{+2.8}_{-2.6} \times 10^{-6}$ [8], suggests that penguins, which dominate here, are large in $B^0 \to \pi\pi$ as well.

These circumstances make the proposal of Snyder and Quinn [3] to use a detailed analysis of the decay $B^0 \to \rho\pi$ for determining α more compelling than ever. The interference between the various $\rho\pi$ bands in the three-pion Dalitz plot would provide valuable information on the phases of the various amplitudes. The amplitudes for the quasi-two-body processes $B \to \rho\pi$ are taken to be complex constants. If we regard the Breit-Wigner form as known, then isospin invariance (violated only by the small electroweak penguin contributions) suffices to isolate the non-penguin amplitudes. In principle this would allow the determination of α, even in the presence of penguin contributions. Monte Carlo simulations by Snyder and Quinn of $B^0 \to \rho\pi$ indicated that 1000 background-free events would be adequate for a measurement α to $\pm 6°$, were it not for the ambiguity between α and $\pi/2 - \alpha$. These two solutions are equivalent if the distribution depends only on $\sin 2\alpha$. In fact, in the full time-dependent Dalitz plot analysis $\cos 2\alpha$ occurs as well. The ambiguity, Snyder and Quinn found, is generally resolved with about 2000 events.

1.3 Results of this Study

We have extended the work of Snyder and Quinn by examining the effects of backgrounds, detector limitations, tagging, uncertainties in the form of the resonant $\pi\pi$ amplitudes and other effects that will inevitably be present in real data. We have examined the influence of penguin amplitudes on the analysis and the potential benefits of untagged data. Of course our simulations of backgrounds have a hypothetical character. We cannot anticipate these, but they will be studied with real data, some of which will be taken off the $\Upsilon(4S)$ resonance.

We have addressed specifically CP measurements that can be made at the asymmetric e^+e^- colliders at SLAC and KEK, but many of our considerations will apply, as well, to experiments at hadron colliders, such as those contemplated by the B-TeV and LHC-b collaborations.

Our primary conclusions are

- The decay $B \to \rho\pi$, as noted in ealier studies, provides a means to determine not just $\sin 2\alpha$, but α itself, up to an amibiguity between α and $\pi + \alpha$. Interference breaks the degeneracy between certain discrete alternative solutions. For the parameters chosen in this study, the most important near degeneracy is between α and $\pi/2 - \alpha$.

- Setting aside the partial ambiguity between α and $\pi/2-\alpha$, in an idealized experiment with N perfectly measured and tagged events and using the decay parameters assumed here, the statistical uncertainty in α is roughly $2/\sqrt{N}$. Studies [4] suggest that reconstruction and tagging (including the correction for mistagging) cost about a factor of one-third each. Each 30 fb^{-1} should produce 1000 to 1800 $B \to \rho\pi$ decays, providing 100 - 200 effectively perfect events.

- In an idealized experiment, the wrong choice between α and $\pi/2 - \alpha$ will be made about 15% of the time with 600 perfect events, but only 5% of the time with 1200 events. This result will be degraded by backgrounds and by uncertainties introduced by other three-pion processes.

- Ignoring penguin contributions can lead to systematic shifts in the derived values of α on the order of 0.15 for the parameters chosen for this study.
- While the shape of the Breit-Wigner associated with the $\rho(770)$ may be well understood, there are likely to be contributions from higher mass $\pi\pi$ resonances. These will interfere with the $\rho(770)$ where there bands cross in the Dalitz plot. This is an important potential source of systematic error.
- Loss of low energy photons or pions depletes the interference regions in the Dalitz plot and degrades the resolving power of the experiment.
- The charged particle momentum resolution and gamma energy and angular resolutions do not substantially impact the analysis.
- Untagged events can contribute to the analysis but their importance depends on the strong phases of the amplitudes.
- If the distributions of the backgrounds in the Dalitz plot are understood they can be included in the analysis with some degradation in precision.

Each of these is discussed in some detail below. **We need to give a brief outline of the paper.**

2 Decay Amplitudes

The quasi-two-body decays $B^0 \to \rho\pi$ and $\overline{B}^0 \to \rho\pi$ require a total of six complex amplitudes to account for the three possible charge combinations in the final state. We take these amplitudes to be constants, independent of the variable mass of the ρ. The full amplitudes for the three-pion final states are obtained by adjoining Breit-Wigner resonant forms and the appropriate angular dependence as described in detail in Appendix A. The six amplitudes represent the maximum information available. In fact one overall phase is unobservable and the overall scale is set by the total decay rate to $\rho\pi$. There are then ten remaining observables.

2.1 Amplitudes for $B^0, \overline{B}^0 \to \rho\pi$

If CP were conserved only three complex amplitudes would be required to describe the decays of neutral B's to $\rho\pi$ since the decay amplitudes for B^0 and $\overline{B}^0$ would be directly related. CP violation introduces phases that are reversed by going from one process to its CP conjugate. Each weak interaction mechanism may have its own CP-violating phase. The B decays to $\rho\pi$ get contributions from both "tree" and "penguin" processes. The amplitudes can be re-expressed in terms of corresponding tree (T) and penguin (P) amplitudes and the unitarity triangle angle α

$$
\begin{array}{rcccccl}
A(B^0 \to \rho^+\pi^-) & \equiv & A^{+-} & = & e^{-i\alpha}T^{+-} & + & P^{+-} \quad , \\
A(B^0 \to \rho^-\pi^+) & \equiv & A^{-+} & = & e^{-i\alpha}T^{-+} & + & P^{-+} \quad , \\
A(B^0 \to \rho^0\pi^0) & \equiv & A^{00} & = & e^{-i\alpha}T^{00} & + & P^{00} \quad , \\
A(\overline{B^0} \to \rho^+\pi^-) & \equiv & \overline{A}^{+-} & = & e^{+i\alpha}T^{-+} & + & P^{-+} \quad , \\
A(\overline{B^0} \to \rho^-\pi^+) & \equiv & \overline{A}^{-+} & = & e^{+i\alpha}T^{+-} & + & P^{+-} \quad , \\
A(\overline{B^0} \to \rho^0\pi^0) & \equiv & \overline{A}^{00} & = & e^{+i\alpha}T^{00} & + & P^{00} \quad .
\end{array}
\tag{1}
$$

The amplitudes for the decay of $\overline{B}^0$ have absorbed the mixing phase, as described in Appendix A. Changing α to $\alpha+\pi$ simply changes the relative signs of the T and P amplitudes. Unless there is a priori knowledge from theory, these alternatives cannot be distinguished. For our purposes it suffices to consider α between 0 and π. Note that in the limit in which CP is conserved $\alpha = 0$, $A^{-+} = \overline{A}^{+-}$, $A^{+-} = \overline{A}^{-+}$, and $A^{00} = \overline{A}^{00}$.

Because the penguin processes are purely $\Delta I = 1/2$ there are only two independent penguin amplitudes [2] and

$$P^{00} = -\tfrac{1}{2}(P^{+-} + P^{-+}). \tag{2}$$

Neglecting one overall phase and the overall scale, there are nine real parameters to fit and ten observables. The constraint imposed by the $\Delta I = 1/2$ character of the penguins can be expressed as

$$\left| \frac{A^{+-} + A^{-+} + 2A^{00}}{\overline{A}^{+-} + \overline{A}^{+-} + 2\overline{A}^{00}} \right| = |e^{-2i\alpha}| = 1, \tag{3}$$

which follows from Eqs. (1) and (2).

Charged-B Decays description

Assuming isospin symmetry and neglecting electroweak penguins (see below), the charged B-decay amplitudes to $\rho\pi$ can be written as [2]:

$$\begin{array}{rclcl}\sqrt{2}\,A(B^+\to\rho^+\pi^0) & \equiv & A^{+0} & = & e^{-i\alpha}T^{+0}+P^{+-}-P^{-+}\,, \\ \sqrt{2}\,A(B^+\to\rho^0\pi^+) & \equiv & A^{0+} & = & e^{-i\alpha}(T^{+-}+T^{-+}+2T^{00}-T^{+0})-P^{+-}+P^{-+}\,.\end{array} \tag{4}$$

Note that there is a pentagonal relation between the five B-decay amplitudes:

$$\sqrt{2}\left(A^{+0}+A^{0+}\right)=A^{+-}+A^{-+}+2A^{00}\,. \tag{5}$$

The addition of the two charged channels $B^{\pm}\to\rho^{\pm}\pi^0\,,\ \pi^{\pm}\rho^0$ in the analysis adds two new theoretical parameters, namely $|T^{+0}|$ and $\mathrm{Arg}(T^{+0})$, and four new observables, namely the two average branching ratios and the two direct *CP*-asymmetries. Therefore the inclusion of these channels could give rather strong constraints on the multi-parameter fit. However the $B^{\pm}\to\rho^{\pm}\pi^0$ channel has two π^0s in the final state, and thus will be more difficult to measure. Without this channel, the other charged decay $B^{\pm}\to\rho^0\pi^{\pm}$ adds as many new parameters as new observables, thus in principal giving no new constraints (though an observation of direct *CP*-violation in the $B^{\pm}\to\pi^{\pm}\pi^+\pi^-$ channel would imply that α is non-zero). Nevertheless, the full three-charged-pion Dalitz plot distribution could give some valuable information on the isospin $I=0,1,2$ resonant and non-resonant contributions and thus should also be considered as a cross-check of the neutral channel Dalitz plot analysis.

2.2 Amplitudes for the three-pion final state

To represent the decay to the full three-pion final state the amplitude for $\rho\to\pi\pi$ consisting of a Breit-Wigner resonance and an angular factor, uniquely determined to be $\cos\theta$ by the decay of a spin-zero particle to a spin-zero particle and a spin-one particle, must be included. The full amplitude includes contributions from all three charge combinations for $\rho\pi$. The interference between these contributions is essential to the analysis. The pertinent amplitudes for B^0 and $\overline{B}^0$ decays are

$$\begin{array}{rcl}\mathcal{A} & = & \cos\theta_+ f(s^+)A^{+-}+\cos\theta_- f(s^-)A^{-+}+\cos\theta_0 f(s^0)A^{00} \\ \overline{\mathcal{A}} & = & \cos\theta_+ f(s^+)\overline{A}^{+-}+\cos\theta_- f(s^-)\overline{A}^{-+}+\cos\theta_0 f(s^0)\overline{A}^{00}\end{array} \tag{6}$$

where s^+, s^-, and s^0 are the invariant masses squared of the dipion systems with charges $+1,-1$, and 0. The function f is the Breit-Wigner resonance form and $\theta_{+,-,0}$ are the $\rho^{+,-,0}$ decay angles, functions of the subenergies, as described in Appendix A.

The time-dependent amplitudes are built from $\mathcal{A}$ and $\overline{\mathcal{A}}$. For the decay of a state initially known to be B^0 at $t=0$ at a later time t we have

$$A_{3\pi}=e^{-\Gamma t/2}[\mathcal{A}\cos\tfrac{1}{2}\Delta mt+i\overline{\mathcal{A}}\sin\tfrac{1}{2}\Delta mt] \tag{7}$$

while for the analogous decay from $\overline{B}^0$

$$\overline{A}_{3\pi}=e^{-\Gamma t/2}[\overline{\mathcal{A}}\cos\tfrac{1}{2}\Delta mt+i\mathcal{A}\sin\tfrac{1}{2}\Delta mt] \tag{8}$$

Resonance (R)	$\mathcal{B}$(R $\to \pi\pi$) (%)	Mass (MeV)	Width (MeV)	$\mathrm{I^G(J^{PC})}$
$\rho(770)$	$\simeq$100	770.9$\pm$ 0.8	150.7$\pm$1.1	$1^+(1^{--})$
$\omega(782)$	2.21	781.94$\pm$0.12	8.43$\pm$.1	$0^-(1^{--})$
$f_0(980)$	(78.1 $\pm$ 2.4)	980$\pm$ 10	40 - 100	$0^+(0^{++})$
$f_2(1270)$	$(84.7^{+2.6}_{-1.2})$	1275$\pm$1.2	$185^{+3.8}_{-2.7}$ 20	$0^+(2^{++})$
$\rho(1450)$	seen	1465$\pm$ 25	310$\pm$ 60	$1^+(1^{--})$
$\rho_3(1690)$	(23.6 $\pm$ 1.3)	1691$\pm$ 5	160$\pm$ 10	$1^+(3^{--})$
$\rho(1700)$	seen	1700$\pm$20	235$\pm$ 50	$1^+(1^{--})$

Table 1: List of some $\pi\pi$ resonances that may contribute to the $B \to 3\pi$ decays [11].

If we regarded the ρ as a stable particle, $\mathcal{A}$ and $\overline{\mathcal{A}}$ would just be fixed complex amplitudes rather than functions of kinematic variables. The decay rates can be written (dropping the exponential decay factor)

$$\begin{aligned}\Gamma(B^0_{phys}(t)) &= \tfrac{1}{2}(|\mathcal{A}|^2+|\overline{\mathcal{A}}|^2)+\tfrac{1}{2}(|\mathcal{A}|^2-|\overline{\mathcal{A}}|^2)\cos\Delta mt+\sin\Delta mt\ \mathrm{Im}\mathcal{A}\overline{\mathcal{A}}^* \\ \Gamma(\overline{B}^0_{phys}(t)) &= \tfrac{1}{2}(|\mathcal{A}|^2+|\overline{\mathcal{A}}|^2)-\tfrac{1}{2}(|\mathcal{A}|^2-|\overline{\mathcal{A}}|^2)\cos\Delta mt-\sin\Delta mt\ \mathrm{Im}\mathcal{A}\overline{\mathcal{A}}^* \end{aligned} \tag{9}$$

2.3 Additional $\pi\pi$ resonances

While the $\rho(770)$ is the most prominent $J=1$ $\pi\pi$ resonance, there are others likely to be seen in $B\to\pi\pi\pi$. The factorization model described in Section 3.2 suggests that one mechanism for the decay is

$$\langle\rho^+\pi^-|J^\mu J_\mu|B^0\rangle \sim \langle\pi^-|J^\mu|B^0\rangle\langle\rho^+|J_\mu|0\rangle \tag{10}$$

The matrix element $\langle\rho^\pm|J_\mu|0\rangle$ is directly observable in the decay $\tau\to\pi\pi\nu_\tau$, while $\langle\rho^0|J_\mu|0\rangle$ is observable (through the isovector electromagnetic current) in e^+e^- annihilation. ALEPH [10] has extracted contributions to the weak vector current from τ decays and from e^+e^- annihilation and parameterized them as a sum of three Breit-Wigner resonances corresponding to the $\rho(770)$, $\rho(1450)$, and $\rho(1700)$

$$f=\frac{f_{\rho(770)}(s)+af_{\rho(1450)}(s)+bf_{\rho(1700)}(s)}{1+a+b} \tag{11}$$

where ALEPH finds for the coefficients a, b, assumed to be real:

$$a = -0.229\pm0.020 \tag{12}$$
$$b = 0.075\pm0.022\ . \tag{13}$$

The actual form used for the Breit Wigner is discussed in Appendix B. In $B\to\pi\pi\pi$ other resonances may appear, as well. A list of some potentially significant $\pi\pi$ resonances is given in Table 1.

In principle, each of the ρ resonances would enter with the same variety of amplitudes as the $\rho(770)$ itself. With our assumption, these amplitudes are simply proportional to the amplitudes for $\rho(770)$ with a constant of proportionality derived from measurements of τ decays and from e^+e^- annihilation. This greatly reduces the number of parameters, but has no deeper justification.

To go further in the study of the impact of unknown resonances in the Dalitz Plot, we also, at times include in the simulation the ρ_3. This resonance is interesting since its spin is different and therefore its $\cos\theta$ dependence is no longer the same as the one of the $\rho(770)$ ($\rho(1450)$ and $\rho(1700)$): the $\cos\theta$ of Eq. (6) is replaced by:

$$\sqrt{\frac{7}{3}}\left(\frac{5}{2}\cos^3\theta - \frac{3}{2}\cos\theta\right) . \tag{14}$$

2.4 Pattern of Interference in the Dalitz Plot

The three-body decay provides the opportunity for interference between different bands of the Dalitz plot. There is interference, too, between B^0 and $\overline{B}^0$ decays caused by oscillations. The squares of the amplitudes in Eqs. (6), (7), and (8) give rise to four categories of terms:

I_0: $|A^{ij}|^2|f^i|^2$,$|\overline{A}^{ij}|^2|f^i|^2$ where $f^i = f(s^i)$ and $i,j = +,-,0$. In the absence of penguins contributions, these squares provide no information on phases.

I_1: $\mathrm{Re}A^{ij}A^{i'j'*}f^i f^{i'*}$, $\mathrm{Re}\overline{A}^{ij}\overline{A}^{i'j'*}f^i f^{i'*}$. These arise from interference between different ρ bands and are not due to oscillations. In the absence of penguins these have no information on α, but do have information on the relative phases of the T's.

I_2: $\mathrm{Im}A^{ij}\overline{A}^{ij*}|f^i|^2$. These are due entirely to oscillations. They carry information on α. In the absence of penguin contributions, for the charged ρs these terms are proportional to $\sin(2\alpha \pm \delta)$, where δ is the relative phase between T^{+-} and T^{-+}. For the neutral ρs they are proportional simply to $\sin 2\alpha$.

I_3: $\mathrm{Im}A^{ij}\overline{A}^{i'j'*}f^i f^{i'*}$. These are the result of the joint action of oscillations and interference of different bands.

The importance of interference can be gauged by its contribution to the square of the matrix element, which varies across the Dalitz plot. [1] We find effects of the order of $\pm 10\%$, even quite far from the ρ-band crossing region [5]. To quantify this we define [5]

Figure 1: *Interference function, ϵ, in the Dalitz Plot. On the left hand side: when both the $\rho(770)$ and the $\rho(1450)$ are present at the generation level. On the right hand side: when the $\rho(770)$ only is present at the generation level.* **I left out the figure here because its file is very large.**

$$\epsilon = \frac{|\sum_i \cos\theta_i f^i|^2}{\sum_i |\cos\theta_i f^i|^2} - 1 , \tag{15}$$

[1] In Ref. [3] a non-relativistic Breit-Wigner is used. It yields significantly stronger interference effects.

where one takes into account only the interference between the different Breit Wigners and the $\cos\theta$ dependence due to the *longitudinal polarization of the* ρ. In Figure 1 we show ϵ for two different data samples: on the left both the $\rho(770)$ and $\rho(1450)$ are present in the generation of events, and on the right only the $\rho(770)$ is present. The very different appearance of the two figures suggests that extra $\pi\pi$ resonances may greatly affect the analysis. The results below bear this out.

2.5 Mirror Solutions

In the absence of penguins, if only $\rho^+\pi^-$ and $\rho^-\pi^+$ are observed and the interference where the bands cross is ignored only the combinations $\sin(2\alpha \pm \delta)$ are determined. In the absence of penguins, this results in ambiguity about the actual values of α and δ, as displayed in Table 2

(α', δ')	$\sin 2\alpha'$	$\cos 2\alpha'$
(α, δ)	$\sin 2\alpha$	$\cos 2\alpha$
$(\pi/4 - \delta/2, \pi/2 - 2\alpha)$	$\cos\delta$	$\sin\delta$
$(\pi/2 + \alpha, \pi + \delta)$	$-\sin 2\alpha$	$-\cos 2\alpha$
$(3\pi/4 - \delta/2, 3\pi/2 - 2\alpha)$	$-\cos\delta$	$-\sin\delta$
$(\pi/4 + \delta/2, -\pi/2 + 2\alpha)$	$\cos\delta$	$-\sin\delta$
$(\pi/2 - \alpha, -\delta)$	$\sin 2\alpha$	$-\cos 2\alpha$
$(3\pi/4 + \delta/2, -3\pi/2 + 2\alpha)$	$-\cos\delta$	$\sin\delta$
$(\pi - \alpha, \pi - \delta)$	$-\sin 2\alpha$	$\cos 2\alpha$

Table 2: List of the 8 mirror solutions (α', δ') for $0 < \alpha < \pi$ when the analysis is made with the assumption that the ρ interferences, the penguin contributions and the $\rho^0\pi^0$ events are negligible. The pairs (α', δ') satisfy $\sin(2\alpha' \pm \delta') = \sin(2\alpha \pm \delta)$.

The degeneracy between these solutions is lifted by the effects we have ignored: interference between the $\rho^+\pi^-$ and $\rho^-\pi^+$ bands, contributions from $\rho^0\pi^0$, and penguin amplitudes. These introduce additional dependence on α. *These dependences split the degeneracies as indicated by the differing values in the last two columns of Table 2.*

If the interference between bands is ignored, only terms of types I_0 and I_2 appear. $\mathrm{Im} A^{ij}\overline{A}^{ij*}$ is invariant under the transformation $A^{ij} \to A^{ij*}, \overline{A}^{ij} \to -\overline{A}^{ij*}$. This is equivalent to changing the relative phases, ϕ_{ij} of A^{ij} and $\overline{A}^{ij}$ to $\pi - \phi_{ij}$. We refer to this as the S transformation. Note that the S-transformed amplitudes still obey the isospin relation, Eq. 2.

These degeneracies are apparent in the "phase space integrated analysis" [5], which ignores $\rho^0\pi^0$ and penguin contributions. Here, interference between $\rho^+\pi^-$ and $\rho^-\pi^+$ is included in an approximate way. Fig. 2 shows χ^2 as a function of α in such an analysis. In addition to the minimum at the input value $\alpha = 1.347$, there are other degenerate minima corresponding to those in Table 2 for $\delta = 0$. The full analysis described below lifts all these degeneracies.

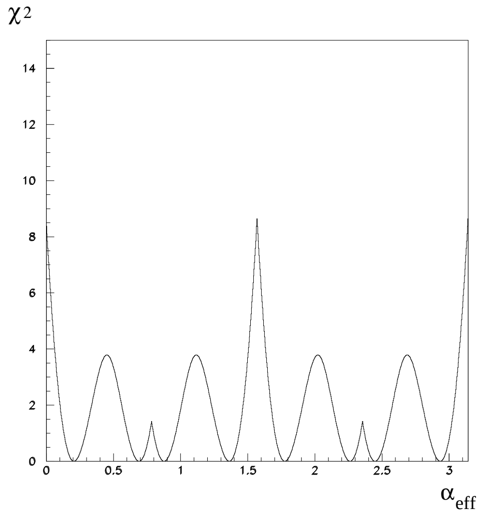

Figure 2: $\chi^2(\alpha)$ vs. α for 1800 signal events generated according to the small penguin scenario described below. The analysis performed to obtain this curve integrates over phase space, and neglects the penguins contributions as well as the $\rho^0\pi^0$. *This analysis cannot split the degeneracies described in Table 2.* Moreover, since penguin contributions are ignored, the analysis is not able to determine the true value of α. It can only establish CP violation through the measurement of a CP-violating parameter α_{eff}, which is not simply related to α. **Did we state that strong phases are set to zero?**

3 Experimental rates and theoretical models

3.1 Observed and anticipated branching ratios

The CLEO Collaboration has reported [8, 9] preliminary results for the branching ratios of neutral and charged B's into $\rho\pi$: $BR(B^0 \to \rho^\pm\pi^\mp) = 3.5^{+1.1}_{-1.0} \pm 0.5 \times 10^{-5}$, $BR(B^+ \to \rho^0\pi^+) = 1.5 \pm 0.5 \pm 0.4 \times 10^{-5}$. With 30 fb^{-1} per year at an asymmetric e^-e^+ collider, this would give 1000 neutral B decays to $\rho\pi$ and 450 charged B decays to $\rho\pi$. Table 3 gives comparisons of anticipated and measured branching ratios and shows corresponding event rates.

Channel	**expected** $\mathcal{B}$ [**4**]	**limits or measurement** (CLEO [**8**],[**9**])	**Expected number of events for 30 fb**$^{-1}$
$B^0 \to \pi^\pm\pi^\mp$	1.0×10^{-5}	$0.47^{+0.18}_{-0.15} \pm 0.13 \times 10^{-5}$	135
$B^0 \to \pi^0\pi^0$	$3. \times 10^{-6}$	$< 0.93 \times 10^{-5}$	15
$B^+ \to \pi^+\pi^0$	$8. \times 10^{-6}$	$< 1.6 \times 10^{-5}$	50
$B^0 \to \rho^\pm\pi^\mp$	5.5×10^{-5}	$3.5^{+1.1}_{-1.0} \pm 0.5 \times 10^{-5}$	350
$B^+ \to \pi^+\rho^0$	1.1×10^{-5}	$(1.5 \pm .5 \pm .4) \times 10^{-5}$	30
$B^0 \to a_1^\pm\pi^\mp$	$6. \times 10^{-5}$	no limit	120
$B^0 \to a_1^0\pi^0$	$3. \times 10^{-5}$	no limit	70
$B^0 \to \rho^+\rho^-$	$5. \times 10^{-5}$	no limit	260
$B^0 \to \rho^0\rho^0$	$5. \times 10^{-5}$	no limit	380

Table 3: Estimated branching ratios for $B \to 2\pi, 3\pi, 4\pi$, [4] and their limits or measurements (at 90% confidence levels) given by CLEO for the channels useful for the determination of α. The fifth column gives the expected number of events for the BaBar detector [4] with 30 fb^{-1} after event-selection and tagging, when one assumes the branching ratios of column 2. No correction has been applied for mistagging.

3.2 Theoretical model for amplitudes

For the purpose of simulations values for all the parameters, T^{+-}, T^{-+}, T^{00}, P^{+-}, P^{-+}, and α are needed. *The value* $\alpha = 1.347$ *has been chosen, consistent with the existing weak constraints.* The amplitudes have been estimated using the factorization assumption, which treats the weak matrix element as a sum of products:

$$\begin{aligned}
\langle\rho^+\pi^-|J^\mu J_\mu|B^0\rangle &\sim \langle\pi^-|J^\mu|B\rangle\langle\rho^+|J_\mu|0\rangle \\
\langle\rho^-\pi^+|J^\mu J_\mu|B^0\rangle &\sim \langle\rho^-|J^\mu|B\rangle\langle\pi^+|J_\mu|0\rangle
\end{aligned} \tag{16}$$

The form factors that are needed are extrapolated from data on $D \to K(K^*)$ [11, 12]. See Appendix B.

The values derived in this way for the tree and penguin diagrams are summarized in the Small Penguin set of Table 4. For the purpose of this analysis, and to study the dependence of the result in the theoretical scenarios at the generator level, we defined two more scenarios: one in which the penguins have been set to zero and another one in which the penguins amplitudes have been enhanced and their phases chosen arbitrarily.

	Small Penguins	**Large Penguins**	**No Penguin**
$\rho + i\eta$	0.05+i0.36	0.05+i0.36	0.05+i0.36
α	1.347	1.347	1.347
T^{+-}	1.00	1.00	1.00
T^{-+}	0.47	0.47	0.47
T^{00}	0.14	0.14	0.14
T^{+0}	1.09	1.09	1.09
P^{+-}	-0.09	$-0.20\, e^{-0.5i}$	0.00
P^{-+}	0.01	$0.15\, e^{2.0i}$	0.00
$B^0 \to \rho^+\pi^-$	4.4×10^{-5}	3.4×10^{-5}	4.4×10^{-5}
$B^0 \to \rho^-\pi^+$	1.0×10^{-5}	0.5×10^{-5}	1.0×10^{-5}
$B^0 \to \rho^0\, \pi^0$	0.1×10^{-5}	0.4×10^{-5}	0.1×10^{-5}
$\overline{B^0} \to \rho^+\pi^-$	1.0×10^{-5}	1.7×10^{-5}	1.0×10^{-5}
$\overline{B^0} \to \rho^-\pi^+$	4.4×10^{-5}	4.9×10^{-5}	4.4×10^{-5}
$\overline{B^0} \to \rho^0\, \pi^0$	0.1×10^{-5}	0.1×10^{-5}	0.1×10^{-5}
$B^+ \to \rho^+\pi^0$	2.6×10^{-5}	2.7×10^{-5}	2.7×10^{-5}
$B^+ \to \rho^0\pi^+$	1.1×10^{-5}	0.9×10^{-5}	1.0×10^{-5}
$B^- \to \rho^-\pi^0$	2.6×10^{-5}	2.4×10^{-5}	2.7×10^{-5}
$B^- \to \rho^0\pi^-$	1.1×10^{-5}	1.2×10^{-5}	1.0×10^{-5}

Table 4: Amplitudes for $B \to \rho\pi$ and expected branching ratios used in the following of the analysis. The phase and the amplitude of the penguin diagrams in the 'large penguin scenario' have been arbitrarily chosen. Recent results from CLEO [9] for the sum of the $\rho^\pm\pi^\mp$ channels give a branching ratio of about 3.5×10^{-5} averaged over B^0 and $\overline{B}^0$. See Table 3. The assumed CKM matrix quantities ρ, η, and α are consistent with existing limits.

Since the $K\pi\pi$ final states introduce a potentially CP-asymmetric background, we also considered the following channels:

- $B^0 \to K^{*+}\pi^-$, with $K^{*+} \to K^+\pi^0$,
- $B^0 \to K^{*0}\pi^0$, with $K^{*0} \to K^+\pi^-$,
- $B^0 \to K^+\rho^-$, with $\rho^- \to \pi^-\pi^0$.

The corresponding branching ratios obtained with the same factorization assumptions are summarized in Table 5.

The amplitudes can be written as follows:

$$A(B^0 \to K^{*+}\pi^-) = T_S^{+-} e^{-i\alpha} + P_S^{+-} e^{i\beta} \,, \tag{17}$$
$$A(B^0 \to \rho^- K^+) = T_S^{-+} e^{-i\alpha} + P_S^{-+} e^{i\beta} \,, \tag{18}$$
$$A(B^0 \to K^{*0}\pi^0) = T_S^{00} e^{-i\alpha} + P_S^{00} e^{i\beta} \,, \tag{19}$$

Channel	Small Penguins	Large Penguins	No Penguin
$B^0 \to K^{*+}\pi^-$	1.1×10^{-5}	3.0×10^{-5}	0.2×10^{-5}
$B^0 \to K^+\rho^-$	0.8×10^{-6}	2.3×10^{-5}	0.8×10^{-6}
$B^0 \to K^{*0}\pi^0$	0.4×10^{-5}	1.8×10^{-5}	0.1×10^{-7}
$\overline{B^0} \to K^{*-}\pi^+$	1.1×10^{-5}	4.7×10^{-5}	0.2×10^{-5}
$\overline{B^0} \to K^-\rho^+$	0.8×10^{-6}	3.9×10^{-5}	0.8×10^{-6}
$\overline{B^0} \to \overline{K}^{*0}\pi^0$	0.4×10^{-5}	1.7×10^{-5}	0.1×10^{-7}
$B^+ \to K^{*+}\pi^0$	0.6×10^{-5}	1.5×10^{-5}	0.1×10^{-5}
$B^+ \to K^+\rho^0$	0.7×10^{-6}	1.1×10^{-5}	0.7×10^{-6}
$B^+ \to K^{*0}\pi^+$	0.7×10^{-5}	3.5×10^{-5}	0
$B^- \to K^{*-}\pi^0$	0.6×10^{-5}	2.4×10^{-5}	0.1×10^{-5}
$B^- \to K^-\rho^0$	0.7×10^{-6}	2.1×10^{-5}	0.7×10^{-6}
$B^- \to \overline{K}^{*0}\pi^-$	0.7×10^{-5}	3.5×10^{-5}	0

Table 5: Estimated branching ratios for the different $K\pi\pi$ final states [4] used in some background simulations.

with the relation:

$$P_{\rm S}^{00} = -\frac{1}{\sqrt{2}} P_{\rm S}^{+-} . \tag{20}$$

3.3 Electroweak Penguins

In addition to the gluonic penguins, there are also Z^0 and photonic penguins, which have different isospin structures, namely a new $\Delta I = 3/2$ contribution proportional to $V_{td}V_{tb}^*$. As a consequence, the relation (2), which is at the core of the isospin analysis is spoiled, and instead *we have*

$$P^{00} + \frac{1}{2}(P^{+-} + P^{-+}) = P_{\rm EW} , \tag{21}$$

where $P_{\rm EW}$ stands for the $\Delta I = 3/2$ electroweak penguin amplitude. Thus there are two new theoretical parameters, namely $|P_{\rm EW}|$ and $\mathrm{Arg}(P_{\rm EW})$, while there is no new observable. Thus the number of parameters exceeds by one unit the number of observables, and the angle α is no longer determined by the three-pion distribution of events.

Because only one hadronic parameter has to be estimated in order to close the system of equations that lead to α, the general method of Ref. [7] may be used to parametrize the electroweak penguin effects in a model-independent way. This is further explained in Appendix C. We do not include electroweak penguins in our analysis and instead regard them as a potential source of systematic error.

4 *Fitting Procedure*

4.1 The Likelihood Function

Using the amplitudes discussed in Section 2, we have simulated $B^0 \to \rho\pi$ and $\overline{B}^0 \to \rho\pi$ decays, including all interference effects with both tree and penguin contributions. The data samples were analyzed using unbinned maximum likelihood to determine the various amplitudes and the angle α. The log-likelihood, $\mathcal{L}$, *was* constructed as the sum over observed events, classifying each event according to the associated tag of the accompanying neutral B. We also did an extended analysis using information from charged B's and from untagged events.

Neutral B decays

The log-likelihood function for perfectly tagged $B \to \rho\pi$ decays can be expressed using the basic formulae of Eqs. (6)-(8):

$$\mathcal{L}^0 = \sum_{B_i^0} \ln \frac{\rho_{3\pi}^i}{\hat{\rho}^0} + \sum_{\overline{B_i^0}} \ln \frac{\overline{\rho}_{3\pi}{}^i}{\hat{\rho}^0}, \tag{22}$$

where

$$\rho_{3\pi}^i = |A_{3\pi}|^2; \qquad \overline{\rho}_{3\pi}^i = |\overline{A}_{3\pi}|^2 \tag{23}$$

evaluated for the values of the momenta and time t of the ith event using Eqs.(6), (7), and (8).

The quantity $\hat{\rho}^0$ is a normalization factor that corresponds to an integration over phase space and time:

$$\hat{\rho}^0 \quad = \quad \int (|A_{3\pi}|^2 + |\overline{A}_{3\pi}|^2) dm^2_{\pi^+\pi^0} dm^2_{\pi^-\pi^0}\ dt\ , \tag{24}$$

where:

$$\int |A_{3\pi}|^2 dm^2_{\pi^+\pi^0} dm^2_{\pi^-\pi^0}\ dt \quad = \quad \int e^{-\Gamma t} (|\mathcal{A}|^2 + |\overline{\mathcal{A}}|^2) dm^2_{\pi^+\pi^0} dm^2_{\pi^-\pi^0} dt \tag{25}$$

The selection efficiencies can be introduced as factors *inside* the phase space integration.

Adding Charged B decays

When we consider, in addition to the neutral B decays, the four charged B channels, the likelihood function takes the following form:

$$\begin{aligned} \mathcal{L} \quad = \quad & \sum_{B^0} \ln \frac{\rho_{3\pi}^i}{\hat{\rho}} + \sum_{\overline{B^0}} \frac{\ln \overline{\rho}_{3\pi}^i}{\hat{\rho}} \\ & + \sum_{B^+} \ln \frac{\rho^{+0}{}_i}{\hat{\rho}} + \sum_{B^+} \ln \frac{\rho^{0+}{}_i}{\hat{\rho}} + \sum_{B^-} \ln \frac{\rho^{-0}{}_i}{\hat{\rho}} + \sum_{B^-} \ln \frac{\rho^{0-}{}_i}{\hat{\rho}} \end{aligned} \tag{26}$$

where ρ^{+0} corresponds to the $\rho^+\pi^0$ state, etc., and where the global normalization factor $\hat{\rho}$ is the sum of the normalization factor for the neutral and the charged B:

$$\hat{\rho} \quad = \quad \hat{\rho}^0 + \hat{\rho}^{+0} + \hat{\rho}^{0+} + \hat{\rho}^{-0} + \hat{\rho}^{0-}\ . \tag{27}$$

The charged B normalization factor reads:

$$
\begin{aligned}
\hat{\rho}^{+0} &= \int |\rho^{+0}|^2 dm^2_{\pi^+\pi^0} dm^2_{\pi^-\pi^0} dt \\
&= |A^{+0}| \int dt \left[\left(\int (|f_1 \cos\theta_1|^2 + |f_2 \cos\theta_2|^2) dm^2_{\pi^+\pi^0} dm^2_{\pi^-\pi^0} \right. \right. \\
&\quad \left. +2Re \int (f_1^+ \cos\theta_1 f_2^{+*} \cos\theta_2) dm^2_{\pi^+\pi^0} dm^2_{\pi^-\pi^0} \ ) \right] .
\end{aligned} \tag{28}
$$

Here the subscripts 1 and 2 refer to the two possible choices for forming the ρ for states like $\pi^+\pi^+\pi^-$.

4.2 Fitting 9 parameters: procedure and mirror solutions

Fitting procedure

Maximization of the log-likelihood was done using MINUIT identifying $\chi^2 = 2(\mathcal{L}_{max} - \mathcal{L})$. A priori, a nine-parameter fit may be expected to present some difficulties. Moreover, we know that in the absence of interference and penguins there are certain to be degenerate maxima. Introducing interference lifts the degeneracies but leaves local maxima in addition to the true global maximum. Indeed, in some data sets, due to fluctuations, a mirror solution will in fact have a higher likelihood than the true solution. As a result, there are two kinds of problems in determining the parameters. The first is to ensure that MINUIT finds the true global solution in the multiparameter space. The second is to translate the log-likelihood as a function of α into a statement of confidence levels. This is an essential issue because we do not in general find the desireable outcome: an isolated solution with a parabolic likelihood function. Instead we often find, especially when the data are not plentiful, two or more solutions with similar χ^2 and a likelihood curve with complicated behavior. A thorough study of this with high statistics simulations has not been undertaken, though we have studied in some circumstances, the frequency with which a mirror solution has a lower χ^2 than the true solution.

To address these problems, we developed a number of strategies, outlined in Appendix D

5 Analysis in the Absence of Background and Detector Effects

In this Section we assume we have in hand a sample of 600 perfectly tagged events. Using the nominal branching ratio for $B \to \rho\pi$ of 5.5×10^{-5} of Ref. [4] there are about 1700 events produced in 30 fb^{-1}. Of these, about 600 would be reconstructed and selected, according to Ref. [4]. If the total tagging efficiency (tagging probability, corrected for the fraction w of wrong tags), $\epsilon(1-2w)^2$ is 0.3, there are effectively 180 pure $B \to \rho\pi$ events in 30 fb^{-1}, so that our sample represents about 100 fb^{-1}. If the central value of the reported branching ratio, 3.5×10^{-5}, is used instead, about 150 fb^{-1} *would be* needed.

Initially, we idealize by ignoring backgrounds and detector limitations. We adopt the large penguin theoretical scenario (cf. Table 4). All three ρ resonances ($\rho(770)$, $\rho(1450)$ and $\rho(1700)$) have been used with the ALEPH parameterization as described in Section 2.3. The relative contributions are fixed at the values obtained by ALEPH.

Each simulated experiment will give a likelihood curve as a function of α. If the number of events in the experiments is large, the differences between the likelihood curves will be slight. For modest statistics, there can be important differences between two experiments. An example of experiment-to-experiment variation of a benign sort is shown in Fig. 3.

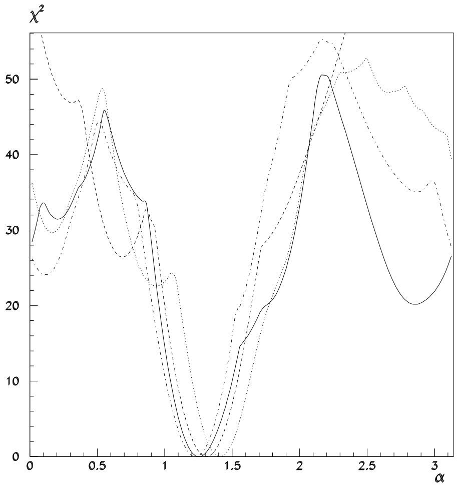

Figure 3: χ^2 as a function of α for different statistics sample: the number of events used in the analysis is constant and equal to 600 perfectly tagged events.

5.1 Illustration of the fit

Fig. 4 shows $\chi^2 = 2(\mathcal{L} - \mathcal{L}_{max})$ as a function of α for two different scenarios: large penguins on the left hand side and small penguins on the right hand side, each for one single experiment of 600 perfect events. The significant difference between the likelihood function for the small and large penguin cases demonstrates the sensitivity of the result to these parameters. One can see that the mirror degeneracies described in Table 2 are lifted. Interference between different ρ bands (see Section 2.4) breaks the degeneracies, but leaves vestigial local minima. While in this

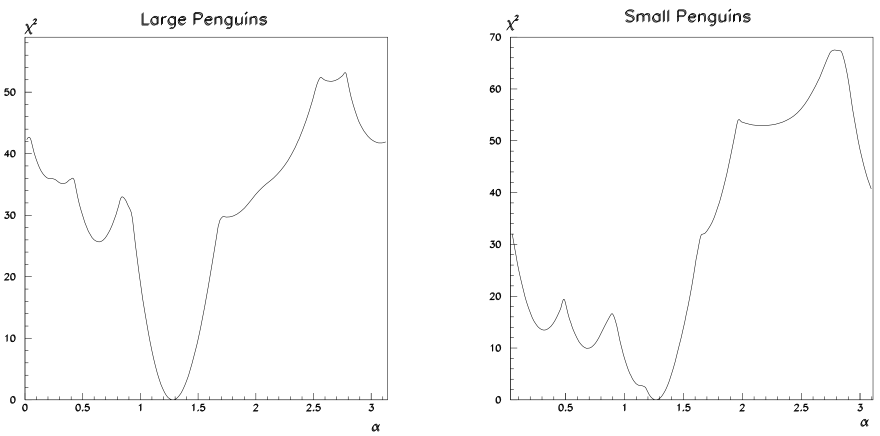

Figure 4: χ^2 as a function of α for the two scenarios: 'Large Penguins' on the left hand side and 'Small Penguins' on the right hand side for 600 perfectly tagged events, without background and detector effects.

example the separation in χ^2 between the true solution and the mirror at $\pi/2-\alpha$ is substantial, this may be an artifact of using the additional ρ resonances. They introduce new interference patterns whose phases we have assumed we know. In practice these won't be known a priori.

As seen in subsequent examples, the separation between the local minima can be so small that for data samples that are not very large, fluctuations can lead to a mirror solution rather than the true solution having the greater likelihood. In these circumstances it is inadequate to look only near the true minimum and gauge the uncertainty in α by a relation like

$$\chi^2(\alpha+\sigma) \quad = \quad \chi^2(\alpha)+1 \ . \tag{29}$$

In the following sections, we will only illustrate the large penguin scenario, and we will refer to the left hand plot in Fig. 4 as the 'reference χ^2'.

5.2 Scanning in α

If we scan in α from 0 to π, at each point fixing α and using MINUIT to find values of the remaining parameters that give the maximum likelihood we find that the results are variable; the local maximum found by MINUIT will depend on the initial values input to the program. These may themselves depend on the solution found for the previous value of α. More picturesquely, using negative log-likelihood, we seek the true minimum and MINUIT may get caught in deep, narrow valleys, from which MINUIT cannot see its way to another, deeper valley. It is necessary to develop strategies that will for each α indeed find the minimum value of $-\mathcal{L}$.

The left hand side of Fig. 5 shows $\chi^2(\alpha)$ for a scan done without looking for mirror solutions, scanning forward from 0 to π in α. The figure on the right hand side shows the same function for the back-scan. One can see that for α around 0.5 the back-scan finds configurations missed by the forward scan. A demonstration that there are valleys in which MINUIT can become emprisoned can be found on the left hand side of Fig. 6 where the two previous χ^2 curves are

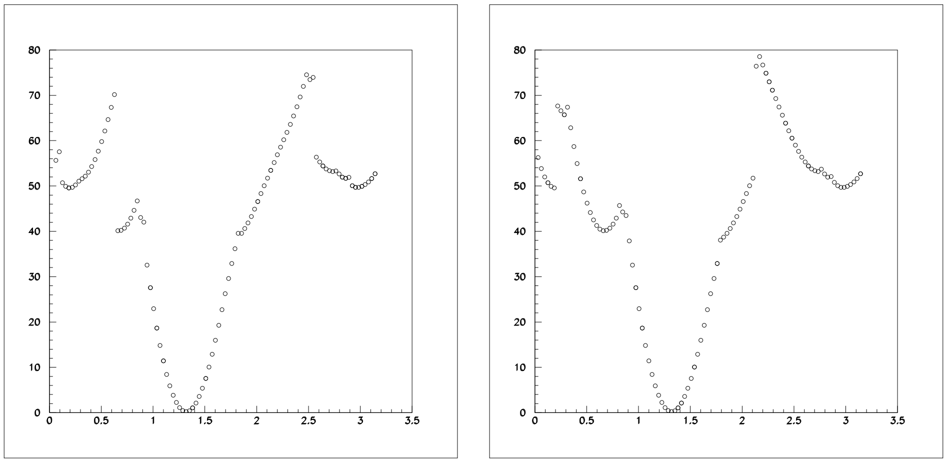

Figure 5: Left: χ^2 as a function of α for a fit done on the basis of a *forward* scan in α only (without search for mirror solution). Right: χ^2 as a function of α for the corresponding back-scan (still without search for mirror solutions).

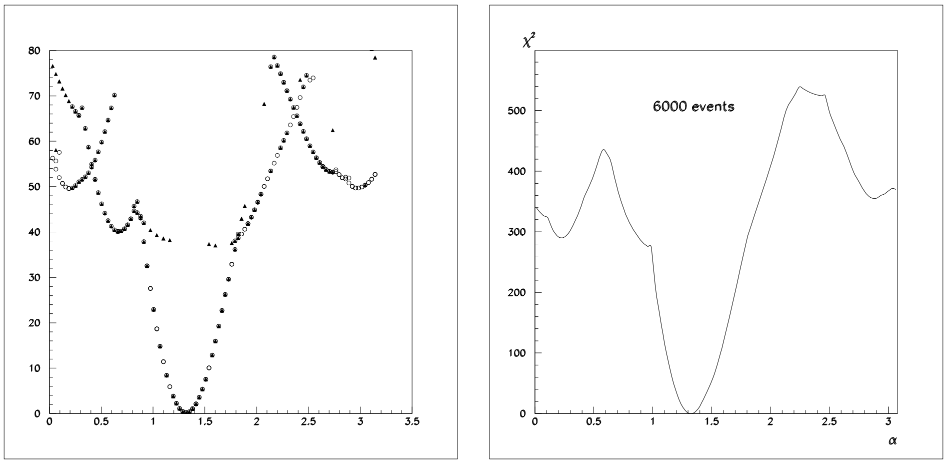

Figure 6: *On the left hand side: superpositions of several* $\chi^2(\alpha)$ *functions for 600 events for several searches for mirror solutions (see text). On the right hand side:* χ^2 *as a function of* α *for 6000 events, when all the mirror solutions have been searched for.*

superposed, in addition to the one obtained when searching carefully for the mirror solutions. Between $\alpha \simeq 1$ and $\alpha \simeq 1.7$, one of the fits follows a valley with $\chi^2 \simeq 40$, which gives a result far from the parabola corresponding to the minimum. The right hand side of Fig. 6,*where 6000 events have been used to suppress statistical fluctuations,* illustrates that $\pi/2 - \alpha$ corresponds to the more resistant degeneracy of the likelihood function. The reason for this is given in Apprendix D.

5.3 Distinguishing the true from the mirror solution

For the parameter set studied here, the most persistent mirror is at $\pi/2-\alpha$. The frequency with which it has a greater likelihood than the true solution decreases as the event sample grows. The results of a study using only the $\rho(770)$ resonance in both the event generation and analysis are shown in Table 6. A sample of 100 Monte Carlo runs has been used.

N_{events}	fraction correct	$\langle\alpha\rangle \pm \sigma$
200	0.70	1.380 ± 0.146
600	0.84	1.369 ± 0.089
1200	0.95	1.360 ± 0.067
10000	1.00	1.348 ± 0.017

Table 6: Monte Carlo determination of α as a function of the number of events in the experiment. The input value was $\alpha = 1.347$ and only the $\rho(770)$ resonance was included. A small shift away from the true value is observed, diminishing as the number of events increases. *The error in α is computed using just the experiments that found the correct, not the mirror, solution.*

The value of σ represents the statistical uncertainty for a sample of this event size. These values are based on 100 runs each with the number of events specified. The shift between the mean value of α found and the input value, 1.347, is statistically significant when N_{events} is small and is evidence for bias, though the bias, $\alpha_{true} - \langle\alpha\rangle$, is in all cases smaller than the intrinsic statistical uncertainty, σ. For example, the 600-event sample has a shift of 0.022 in α, but a statistical uncertainty of 0.089. The fraction of the events in which the minimum of the negative log-likelihood is near the true rather than mirror solution is indicated. As anticipated, with increasing numbers of events, the probability of getting the wrong solution disappears. The spread σ is determined using only "correct" solutions.

Monte Carlo simulations for the large penguin amplitudes considered here indeed find a local minimum of the negative log-likelihood near the mirror obtained by applying the S transformation*(see Section 2.5 and Appendix D)* to the true amplitudes. See Table 7.

The value of $\langle\mathcal{L}\rangle$ is proportional to the number of events N for large numbers of events. The expectation value of the likelihood difference between the true and mirror solutions, $\mathcal{L}_0 - \mathcal{L}_m$ is also proportional to N. This difference varies from experiment to experiment, with a mean $\langle\mathcal{L}_0 - \mathcal{L}_m\rangle$ and a width σ, proportional to $\sqrt{N}$. Simulations using only the $B \to \rho(770)\pi$ show that

$$\langle\mathcal{L}_0 - \mathcal{L}_m\rangle \quad = \quad 1.05 \times 10^{-2} N$$

Amplitudes	True solution	Found mirror	S mirror
ReA^{+-}	1.000	1.000	1.000
ImA^{+-}	0.000	0.000	0.000
ReA^{-+}	0.368	0.363	0.368
ImA^{-+}	0.029	-0.012	-0.029
ReA^{00}	0.295	0.297	0.295
ImA^{00}	0.155	-0.192	-0.155
Re$\overline{A}^{+-}$	-0.672	0.687	0.672
Im$\overline{A}^{+-}$	0.083	0.157	0.083
Re$\overline{A}^{-+}$	-1.212	1.226	1.212
Im$\overline{A}^{-+}$	0.116	0.092	0.116
Re$\overline{A}^{00}$	-0.014	0.015	0.014
Im$\overline{A}^{00}$	0.171	0.108	0.171

Table 7: The true amplitude *used* in the simulations, compared with the *mirror* amplitude found by the Monte Carlo and MINUIT routines, and with the mirror solution defined by applying the S transformation ($A^{ij} \to A^{ij*}$, $\overline{A}^{ij} \to -\overline{A}^{ij*}$) to the original amplitude. The found mirror is a local minimum of the log-likelihood.

$$\langle\sigma\rangle \quad = \quad 0.19\sqrt{N} \tag{30}$$

While $\langle\mathcal{L}_0 - \mathcal{L}_m\rangle$ can be read from the curve showing the likelihood as a function of α, σ cannot. It depends on correlations between the likelihood at true α and the likelihood at the mirror near $\pi/2 - \alpha$. The statistical power for separating the two solutions is indicated by

$$\langle\mathcal{L}_0 - \mathcal{L}_m\rangle/\langle\sigma\rangle = 5.5 \times 10^{-2}\sqrt{N} \tag{31}$$

Thus 600 events would give, on average, 1.3 σ separation. This is in rough agreement with the percentage shown in Table 6. These particular values depend very much on the amplitudes assumed. The separation is degraded by many factors, including backgrounds, limitations in the detector, and tagging inefficiencies.

5.4 Towards Confidence Levels

If experiment were able to determine only $\sin 2\alpha$ it would suffice to quote a value and its uncertainty. In $B \to \rho\pi$ it is α itself that is obtained when the statistics are great enough. However, with limited statistics ambiguities remain, as shown in Table 6, where the fraction of "wrong answers" is displayed as a function of the sample size.

Comparing the right hand side of Fig. 4 and the left hand side of Fig. 7 demonstrates the same point, the difference between the two χ^2 curves coming from the number of events (600 for the first one and 100 for the second). The extraction of a measurement of the form $\alpha \pm \sigma[\alpha]$ from the second example is impossible. Moreover, the separation in χ^2 between the local minima is only a crude guide to the probability that the "wrong answer" will be chosen.

In this circumstance it will be difficult to provide a simple measure of uncertainty of a measurement of α. The curvature of the χ^2 function is certainly no more than a partial reflection of the true uncertainty. The full curve of χ^2 as a function of α comes much closer to expressing the uncertainty, but is still not complete because it does not reflect correlations between the likelihood function evaluated at two different values of α.

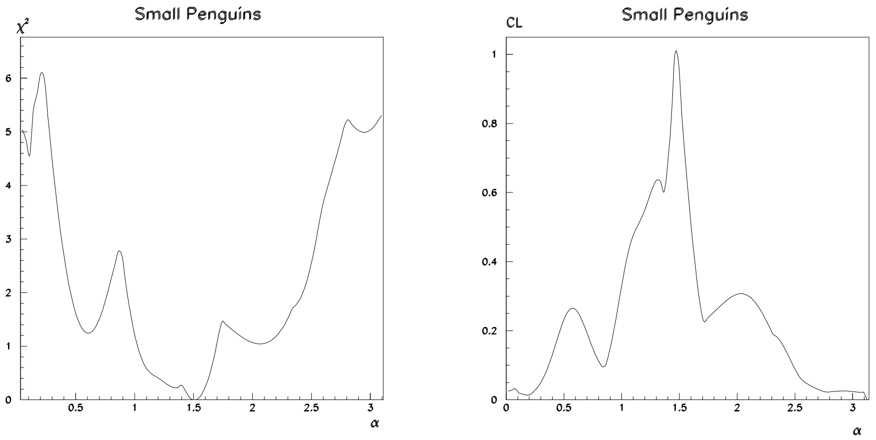

Figure 7: χ^2 (on the left hand side) and corresponding confidence level curve (on the right hand side) as a function of α for the 'Small Penguins' scenario with 100 perfectly tagged events with no background nor detector effects.

5.5 Ignoring Penguins

The difficulty of working with so many independent amplitudes would be lessened if it were possible to ignore the contribution of penguin amplitudes. This, not surprisingly, turns out not to be a reliable procedure in the case of the large penguin amplitudes used in our simulation. This is illustrated in Fig. 8, where χ^2 is shown as a function of α for a 600-event experiment, with the penguin amplitudes set to zero in the analysis. While the reduction of the number of real parameters to be fit to five is attractive, the minimum occurs at the wrong value of α.

Recall that large values of the penguin amplitudes were introduced in response to the larger branching ratios found by CLEO for $B \to K\pi$ than for $B \to \pi\pi$. To estimate the systematic error that might be introduced by ignoring penguin amplitudes in the analysis, events were generated using the large penguin amplitudes, but the analysis was done fixing their values to zero. Many experiments of the size indicated were simulated. Results are shown in Table 5.5.

We see a marked shift of the result obtained ignoring penguins from the true value, $\alpha = 1.347$. The apparent decrease in the uncertainty in α is illusory, a consequence of reducing the number of variables in the fit. The actual shift resulting from ignoring penguins depends in detail on the input amplitudes. A study in which the phases of the amplitudes were varied showed that the shift is typically about half of that observed here, though it can have either sign.[4]

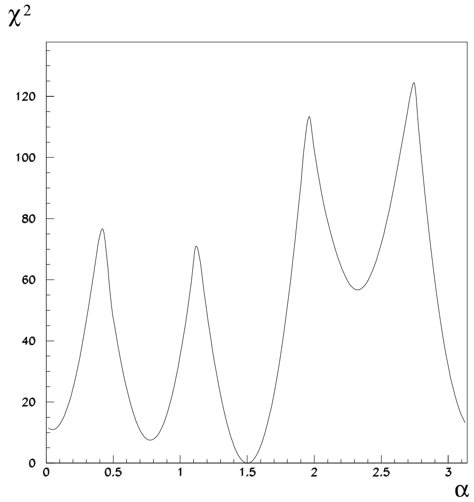

Figure 8: $\chi^2(\alpha)$ *with penguin contributions ignored in the analysis: the number of parameters to fit therefore goes down to 5.*

	Penguins analyzed		Penguins ignored	
N_{events}	fraction correct	$\langle\alpha\rangle \pm \sigma$	fraction correct	$\langle\alpha\rangle \pm \sigma$
200	0.70	1.380 ± 0.131	0.65	1.474 ± 0.068
600	0.84	1.369 ± 0.088	0.81	1.476 ± 0.039
1200	0.95	1.360 ± 0.066	0.91	1.481 ± 0.029

Table 8: Monte Carlo comparison of results of analyzes with and without penguin amplitudes. In both cases the events were generated with the large penguin amplitudes. A large shift away from the input value $\alpha = 1.347$ is seen. Mirror solutions were ignored in determining the mean value of α. The small apparent uncertainty in α in the analysis without penguins is illusory since the value of α itself is wrong. The systematic error introduced by the approximation depends on the sizes and phases of the tree and penguin amplitudes.

5.6 Neglecting strong phases

5.7 Effect of our knowledge of the $\rho(1450)$

As described in Section 2.3, additional $\pi\pi$ resonances are expected to occur in the $B \to 3\pi$ decay. If the $J = 1$ $\pi\pi$ resonance is factored and coupled to the weak current, then result from $\tau^+ \to \ell^+\nu\pi\pi$ can be used directly. However, this is not the only way that the $\pi\pi$ system can be coupled in B decay. The most general form would introduce as many new amplitudes for $B \to \rho(1450)\pi$ as there are for $B \to \rho(770)\pi$. To avoid this, we have made the assumption that all the $B \to \rho(1450)\pi$ amplitudes are proportional to those for $B \to \rho(1450)\pi$, leaving a single overall proportionality factor (which we take to be real) to be determined. This gives an enormous simplification, but must be recognized as an unsupported assumption.

When one band from $\rho(14500)$ and one from $\rho(770)$ intersect, there will be important interference effects. Failing to treat the effects properly could introduce an important systematic error. The pattern of these interference effects is shown in Fig. 1. There we see the marked difference that excluding the $\rho(1450)$ would make.

This is borne out by a study made by applying cuts to isolate the $\rho(770)$. Three different sets of cuts have been used to select the $\rho(770)$ band: the usual BaBar selection for which the invariant mass lies in the range 0.1225 GeV^2 $< m^2_{\pi\pi} <$ 1.44 GeV^2 which is denoted as large, and two other ones: 0.33 GeV^2 $< m^2_{\pi\pi} <$ 1.21 GeV^2 (medium) and 0.44 GeV^2 $< m^2_{\pi\pi} <$ 1.1 GeV^2 (tight). The impact of these cuts is shown in Fig. 9. These likelihood curves bear little resemblance to the reference curve. After the cuts, the effects of the $\rho(1450)$ remain from the overlap between the two resonance bands. Cutting on the $\rho(770)$ does not remove the consequences of the $\rho(1450)$.

$\rho(770)$ selection

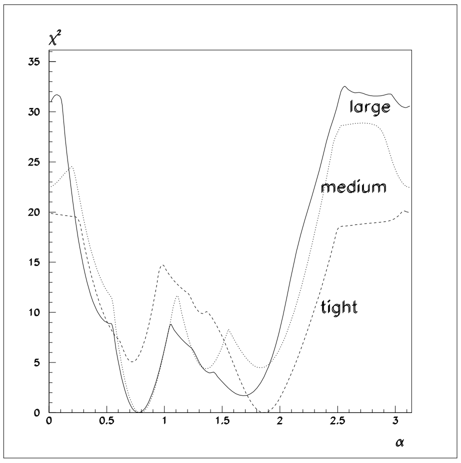

Figure 9: *χ^2 as a function of α when one neglects the $\rho(1450)$ in the fit and makes use of three kinds of cuts: large, medium and tight to select the $\rho(770)$ band (see text for more details on the cuts). There are 600 3π-events used passing the cuts in each case.*

N_{events}	fraction true	$\langle\alpha\rangle \pm \sigma$	$\langle a_{1450}\rangle \pm \sigma$
200	0.95	1.364 ± 0.102	-0.230 ± 0.023
600	1.00	1.351 ± 0.076	-0.226 ± 0.015

Table 9: Monte Carlo results on determining the contribution from $\rho(1450)$. All the amplitudes for $B \to \rho(1450)\pi$ are taken to be proportional to those for $B \to \rho(770)\pi$. The overall real constant of proportionality is $a_{1450} = -0.228$ in the simulation. See Eq. (11). It is seen to be well determined by the fit.

Fitting for the $\rho(1450)$ contribution

A clear alternative to cutting on the ρ mass is to include the $\rho(1450)$ in the fit, with its contribution a free parameter. If we adopt the philosophy of making the $\rho(1450)$ contribution to the amplitude the same as that of the $\rho(770)$ except for a real scale factor, this introduces just one new real parameter. The ALEPH measurements of $\tau^+ \to \ell^+\nu\pi\pi$ indicated that the $\rho(1450)$ entered the weak vector current with a factor -0.228 relative to that of the $\rho(770)$. Using this value to generate events, and using Minuit to fit for the best value of this coefficient, a_{1450}, the results shown in Table 5.7 were obtained.

The Table shows that the presence of the $\rho(1450)$ appears not to be a problem. It even seems to improve the results. This is an artifact of our assumptions. By taking the $\rho(1450)$ to introduce only a single new real parameter, actually more information is gained from the $\rho(1450)$ data than is required to compensate for the new uncertainty.

5.8 Effect of poorly known resonances

Given the impact of the $\rho(1450)$, one may wonder about other resonances (cf. Table 1). We are going to focus in the following sections on three of them: the $\rho(1700)$ since it is close to the $\rho(1450)$,*the* $\rho_3(1690)$ *since its spin is different, giving a different* $\cos\theta$ *dependence, and finally the* $f_0(980)$ *since it is very close to the* ρ^0 *band.*

The $\rho(1700)$

The ρ_3

If we use $\cos\theta$ as the angular distribution, this isn't a ρ_3. It is just another version of $\rho(1700)$. Figure 11 shows the effect of the ρ_3 on curve (2) when its contribution is set to 0.2 and on curve (3) with a contribution of 0.2 and the $\cos\theta$ dependence of the $\rho(770)$. The analysis is performed neglecting the ρ_3 in the Breit Wigner description, and cutting on the $\rho(770)$ bands. The amplitudes of the χ^2 are low and the mirror solutions go down: without including the ρ_3 in the analysis, one dilutes/bias the information dramatically. This is the same effect than for the $\rho(1700)$.

The f_0

5.9 Electroweak penguins

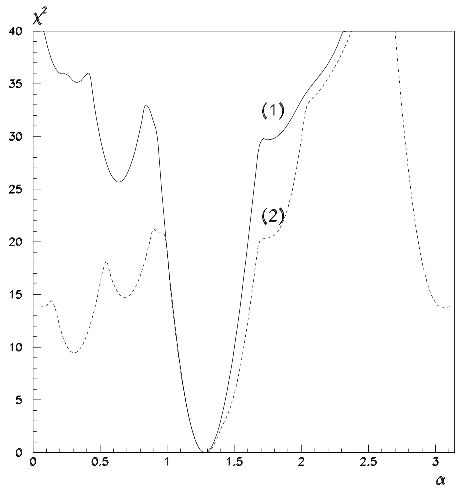

Figure 10: *Curve (1) is the reference, without cuts. Curve (2) shows the effect of ignoring the* $\rho(1700)$ *in the analysis. The events are all generated using the* $\rho(770)$, $\rho(1450)$, *and* $\rho(1700)$ *with the parameters found by the ALEPH Collaboration.*

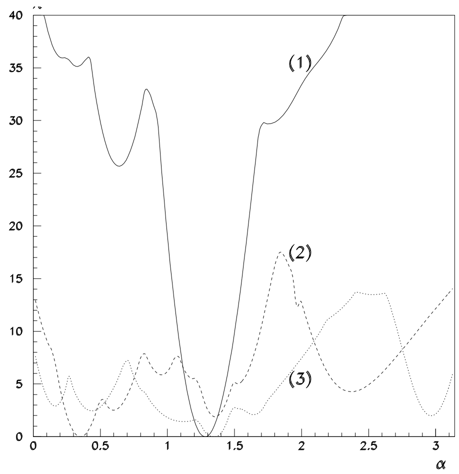

Figure 11: $\chi^2(\alpha)$ *for 600 events in the Large Penguins scenario. The curve (1) represents the reference* χ^2, *curve (2) corresponds to a 0.2 contribution of the* ρ_3 *and curve (3) corresponds to a 0.2 contribution of the* ρ_3 *with the* $\cos\theta$ *dependence of the* $\rho(770)$.

6 Backgrounds, Tagging, and Efficiencies

We consider here the practical limitations imposed by a detector, taking as an example the BaBar experiment [13][4], though similar considerations would apply to any experiment at an asymmetric B factory. The issues will be somewhat different at hadron colliders, which we consider briefly.

6.1 Impact of acceptance cuts

Description of the cuts

To study the effects of detector acceptance cuts, we use the two sets – pessimistic and optimistic – described in Table 10, which gives the rejection efficiencies for each. Some cuts are due to the detector design and performance. Others, like the cut on the invariant mass of two pions near the $\rho(770)$ bands in the Dalitz plot, are intended to enhance the signal . Such cuts do, however, remove information, in this case lessening control over the backgrounds that vary continuously across the plot.

Pessimistic cuts	**Rejection**	**Optimistic cuts**	**Rejection**
θ_{accept}	18.0%	θ_{accept}	18.0%
$E_\gamma > 50$ MeV	11.0%	$E_\gamma > 25$ MeV	3.0%
$P_T > 100$ MeV	6.0%	$P_T > 50$ MeV	2.0%
$\mathrm{m}^2(\pi\pi)$	0.04%	$\mathrm{m}^2(\pi\pi)$	0.04%
Total	33.3%	Total	24.8%

Table 10: Description of the two set of cuts used in the analysis of $B \to 3\pi$ channel. For both the optimistic and pessimistic sets, the cut on θ is $\pi - 350$ mrad $> \theta_{\text{accept}} > 500$ mrad. In both cases, the cut on $m^2(\pi\pi)$ is $0.12\ \text{GeV}^2 < \mathrm{m}^2(\pi\pi) < 1.44\ \text{GeV}^2$. The rejection percentages are also shown here. **I still don't believe the value 0.04%. I will wager a jambon et gruyere sandwich it is incorrect.**

It was shown in [4] that the combinatorial background in this channel was high (there are about 10 possibilities for each event) due to low energy photons, coming either from the machine background or from the decay of the other B (at BaBar the Bs are produced in pairs). For this purpose we study here two kinds of cuts on the photon energy: $E_\gamma > 25$ MeV and $E_\gamma > 50$ MeV.

In studying the consequences of cuts, we have chosen to fix the number of events that pass those cuts to see how the cuts may bias the analysis. The loss of statistics due to the cuts is a separate matter. See [5].

The χ^2 curves on the left hand side of Fig. 12 shows the effect of the cut on $m^2(\pi\pi)$. The solid curve is the reference one, and the dotted line shows the effect of the cut. The loss of information is not crucial for the analysis: the resolution on α at the minimum is not affected and the differences between the principal minimum and the mirror are not big.

The χ^2 curves on the right hand side of the figure shows the effects of all the cuts: for the optimistic ones in (2) and for the pessimistic ones in (3). Since the difference between the two

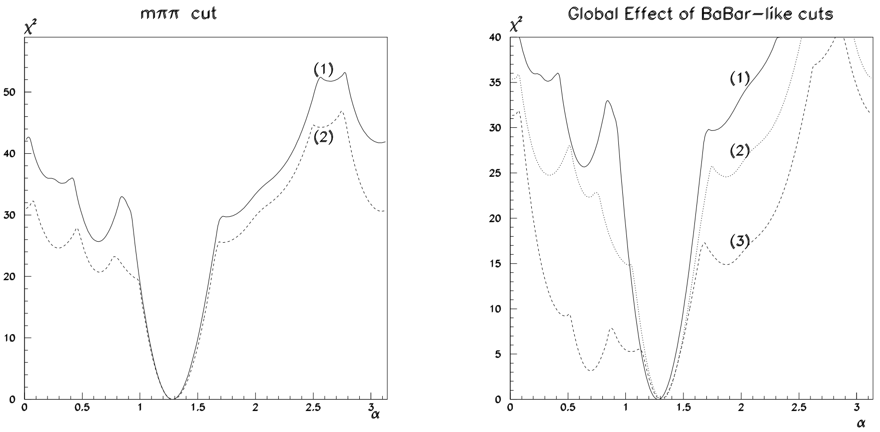

Figure 12: *On the left hand side: effect of the cut on $m^2(\pi\pi)$. The function number (1) corresponds to the reference χ^2 and the number (2) illustrates the impact of the cut. On the right hand side: effect of the two sets of cuts described in table 10. Curve (1) is still the reference; curve (2) corresponds to the optimistic set of cuts and curve (3) to the pessimistic set. The number of events passing the cuts is 600.*

set of cuts comes only from the threshold in the photon energy, it is clear that this threshold is of critical importance. In the pessimistic case, the principal mirror solution goes down to a level where it may become difficult to distinguish it from the principal minimum even with 600 reconstructed and tagged events. The loss of low energy photons cuts away the overlap between the ρ^+ and ρ^- bands where crucial information on interference lies.

LHC-B-like cuts

The cuts that might be imposed by LHC-B [14], a dedicated B physics experiment under development for the Large Hadron Collider at CERN, differ from ones at an asymmetric e^+e^- collider. LHC-B event selection for 3π would remove most of the events at the corner of the ρ^+ and ρ^- bands as is shown on the left hand side of figure 13[14]. The effect is similar in kind to the loss of low energy photons at BaBar, but more severe. The extraction of α is affected by such a cut as seen from curve (2) on the right hand side of Fig. 13. The figure shows results from 600 events, while LHC-B samples should be many times as large.

6.2 Impact of the detector resolution

Description of the resolution

To evaluate the effect of detector resolution on the analysis of $B \to \rho\pi$, we use values anticipated for the BaBar detector [4]. The estimates of the resolution on the transverse momentum for charged pions, on the photon energy and on the angular resolution of γs are taken to be:

$$\sigma(P_\perp) = 0.3\%\ P_\perp \tag{32}$$

$$\frac{\sigma_E}{E} = \frac{1\%}{\sqrt[4]{E(\mathrm{GeV})}} \oplus 1.2\% \tag{33}$$

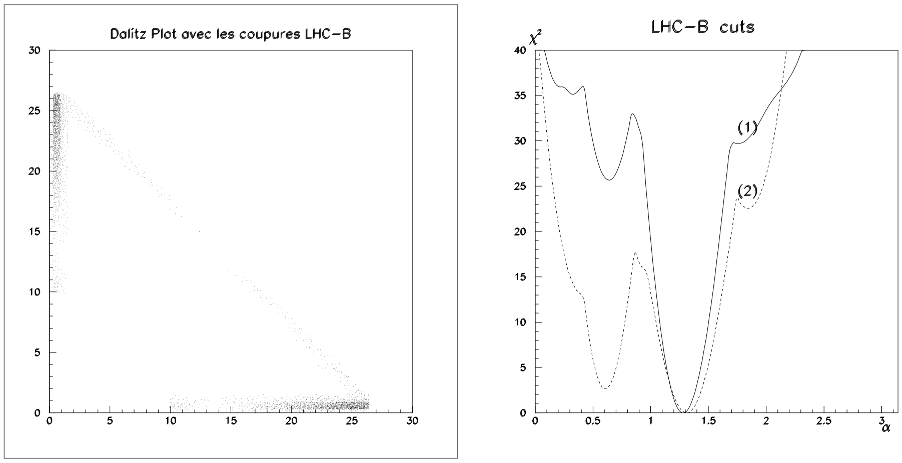

Figure 13: *On the left hand side: simulation of a LHC-B-like cut in the Dalitz Plot. On the right hand side: χ^2 as a function of α for 600 events: the curve (1) is the reference, and curve (2) demonstrates the effects of the cut shown on the left. The event selection has removed the region of overlap between $\rho^+\pi^-$ and $\rho^-\pi^+$.*

$$\sigma_{\theta,\phi} = \frac{3 \text{ mrad}}{\sqrt{E(\text{GeV})}} \oplus 2 \text{ mrad} . \tag{34}$$

If a $\pi\pi$ pair is close to the peak of the Breit-Wigner, mismeasurement of the invariant mass will lead to a change in the phase of the amplitude. The resolution of $m_{\pi\pi}$ in the region of the ρ resonance has been estimated by Monte Carlo with the result $\sigma(m_{\pi\pi}) \approx 0.015$ GeV. This is sufficiently small compared to the width of the ρ to suggest that resolution will not be a problem. This has been verified by Monte Carlo simulation, as shown in Fig. 14.

6.3 Impact of our knowledge of selection efficiencies

Effect on the α extraction

6.4 Impact of B-Tagging

While untagged data can provide information on direct CP violation (for example, the difference between $\Gamma(B^0 \to \rho^+\pi^-)+\Gamma(\overline{B}^0 \to \rho^+\pi^-)$ and $\Gamma(B^0 \to \rho^-\pi^+)+\Gamma(\overline{B}^0 \to \rho^-\pi^+)$, the most incisive results come from tagged data. In two-body decays like $B \to J/\psi K_S$, the tagging efficiency ϵ and wrong-tag probability w effectively reduce the number of reconstructed events from N to $\epsilon(1-2w)^2 N$. For three-body decays like $B \to \rho\pi$ this is not necessarily so. The untagged events carry information about the decay amplitudes, which may help constrain the overall fit. In particular, untagged events can help separate the true and mirror solutions.

If A and A' are interfering amplitudes for B^0 decay and $\overline{A}$ and $\overline{A}'$ are the corresponding amplitudes for $\overline{B}^0$ decay, in general we have expressions like

$$|\cos\tfrac{1}{2}\Delta mt(Af + A'f') + i\sin\tfrac{1}{2}\Delta mt(\overline{A}f + \overline{A}'f')|^2 \tag{35}$$

opposite a $\overline{B}^0$ tag and

$$|\cos\tfrac{1}{2}\Delta mt(\overline{A}f + \overline{A}'f') + i\sin\tfrac{1}{2}\Delta mt(Af + A'f')|^2 \tag{36}$$

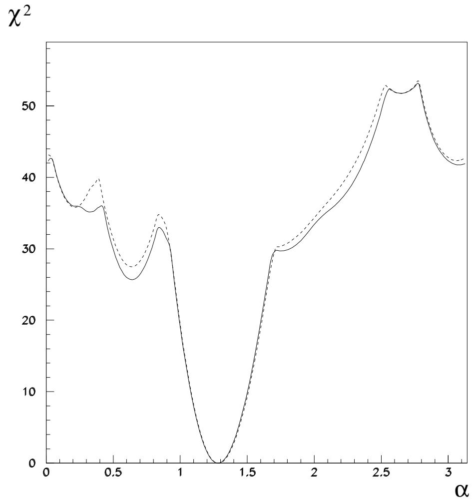

Figure 14: The full curve corresponds to the reference χ^2 and the dashed curve represents the χ^2 obtained after having added in the simulation the resolution effects of the detector. No other limitations are considered. It is apparent that there is little loss in information expected from the detector resolution performance.

opposite a B^0 tag, where as discussed earlier, the phase from mixing has been conveniently absorbed into the definitions of $A, A', \overline{A}$ and $\overline{A}'$.

Untagged data never show the effect of mixing: there are no bilinears involving amplitudes from both B^0 and $\overline{B}^0$, as can be seen by adding Eqs. (35) and (36) . Thus untagged data are described entirely by expressions of the types I_0 and I_1 described in Section 2.4.

The greatest potential value of the untagged data is in distinguishing the true solution α from the mirror solution $\pi/2 - \alpha$. The corresponding contributions from the mirror solutions obtained by the S $(A \to A^*, \overline{A} \to -\overline{A}^*)$ transformation are, for the B^0 and $\overline{B}^0$ tags, respectively,

$$\begin{aligned}
&|\cos\tfrac{1}{2}\Delta mt(A^*f + A'^*f') - i\sin\tfrac{1}{2}\Delta mt(\overline{A}^*f + \overline{A}'^*f')|^2 = \\
&\qquad |\cos\tfrac{1}{2}\Delta mt(Af^* + A'f'^*) + i\sin\tfrac{1}{2}\Delta mt(\overline{A}f^* + \overline{A}'f'^*)|^2; \\
&|\cos\tfrac{1}{2}\Delta mt(\overline{A}^*f + \overline{A}'^*f') - i\sin\tfrac{1}{2}\Delta mt(A^*f + A'^*f')|^2 = \\
&\qquad |\cos\tfrac{1}{2}\Delta mt(\overline{A}f^* + \overline{A}'f'^*) + i\sin\tfrac{1}{2}\Delta mt(Af^* + A'f'^*)|^2
\end{aligned} \tag{37}$$

The difference between the true and mirror solutions is, again for the B^0 and $\overline{B}^0$ tags, respectively,

$$\begin{aligned}
&2[-(\cos\tfrac{1}{2}\Delta mt)^2\mathrm{Im}AA'^* - (\sin\tfrac{1}{2}\Delta mt)^2\mathrm{Im}\overline{A}\overline{A}'^* + \sin\tfrac{1}{2}\Delta mt\cos\tfrac{1}{2}\Delta mt\mathrm{Re}(A\overline{A}'^* - A'\overline{A}*)]2\mathrm{Im}ff'^*; \\
&2[-(\cos\tfrac{1}{2}\Delta mt)^2\mathrm{Im}\overline{A}\overline{A}'^* - (\sin\tfrac{1}{2}\Delta mt)^2\mathrm{Im}AA'^* - \sin\tfrac{1}{2}\Delta mt\cos\tfrac{1}{2}\Delta mt\mathrm{Re}(\overline{A}A'^* - A'\overline{A}*)]2\mathrm{Im}ff'^*
\end{aligned} \tag{38}$$

Tagged data are sensitive to all of these terms. Untagged data see only the sums of the terms of the form AA'^* and $\overline{A}\overline{A}'^*$. These occur only as $\mathrm{Im}(AA'^* + \overline{A}\overline{A}'^*)$. In the example considered here,

quantity	perfect events	tagged and untagged events	tagged events only
$\langle \mathcal{L}_0 - \mathcal{L}_m \rangle / N$	0.0091	0.0029	0.0026
$\sigma / \sqrt{N}$	0.17	0.11	0.11
$(\langle \mathcal{L}_0 - \mathcal{L}_m \rangle / \sigma) / \sqrt{N}$	0.053	0.026	0.024

Table 11: The likelihood difference between the true and mirror solutions as found by Monte Carlo simulations, using typically ten 10,000-event experiments. The amplitudes used were the standard large penguin amplitudes defined above. The tagging efficiency was taken to be $\epsilon = 0.6$ and the wrong tag probability was taken to be $w = 0.15$. The naive expectation that the effective efficiency would be $\epsilon(1-2w)^2 = 0.29$ is supported here. The untagged data have little power to discriminate between the true and mirror solutions.

as seen in Table 7, the dominant amplitudes are relatively real. Thus the untagged data are not especially effective in helping to break the degeneracy between the true and mirror solutions. Numerical results are shown in Table 11. We see that the separation per event is indeed reduced by just about the factor $\epsilon(1-2w)^2 = 0.29$ anticipated, indicating that little has been derived from the untagged or wrongly tagged events, at least as applies to distinguishing between the real and mirror solutions.

These results are quite specific to the values assumed for the amplitudes. To obtain some idea of the variability of this behavior, similar calculations were done with the amplitudes obtained by multiplying the value of T^{-+} by i. The results are shown in Table 12

quantity	perfect events	tagged and untagged events	tagged events only
$\langle \mathcal{L}_0 - \mathcal{L}_m \rangle / N$	0.0248	0.0085	0.0070
$\sigma / \sqrt{N}$	0.32	0.12	0.13
$(\langle \mathcal{L}_0 - \mathcal{L}_m \rangle / \sigma) / \sqrt{N}$	0.078	0.069	0.054

Table 12: The likelihood difference between the true and mirror solutions as found by Monte Carlo simulations, using typically ten 10,000-event experiments. The amplitudes used were the standard large penguin amplitudes, except that T^{+-} was multiplied by i. The tagging efficiency was taken to be $\epsilon = 0.6$ and the wrong tag probability was taken to be $w = 0.15$. The naive expectation that the effecive efficiency would be $\epsilon(1-2w)^2 = 0.29$ is not supported here. The untagged and wrong tagged events provide information that is ultimately useful in determining α.

As anticipated, the effectiveness of the untagged events increases when the dominant amplitudes are not relatively real. Adding the wrongly-tagged and untagged events decreases variability in the difference in likelihood between the true and mirror solutions. The naive expectation that σ would be proportional to $\sqrt{\epsilon}(1-2w)$ fails because of extra information in the added events.

6.5 Impact of $B\bar{B}$ and $q\bar{q}$ backgrounds

Description of the expected background

Earlier studies [4] found that of 1000 produced $\rho\pi$ events (requiring roughly 30 fb^{-1}) about 600 would be reconstructed (without tagging), and that about 2000 $q\overline{q}$ background events might be reconstructed as $\rho\pi$ in the ρ region in the same sample. Tagging would reduce these numbers to about 350 signal and 590 background. Other sorts of events – $B\bar{B}$ and as well as $K\pi\pi$ – may further dilute the signal.

In the following discussions on the impact of background, we do not assume the background over signal ratio B/S to be known: we have to fit it and therefore have to perform a ten-parameter fit. As the $\rho^0\pi^0$ is expected to be color-suppressed, the background obscures this band in particular.

Background study with restriction to the ρ bands

One approach to the backgrounds due to $q\overline{q}$ events is to restrict attention to the actual ρ bands. The background differs from the signal in that it lacks the characteristic $\cos^2\theta$ behavior. In addition, the $q\overline{q}$ background will have a very different time (i.e. Δz) behavior from that of the signal.

We have simulated the $q\overline{q}$ background in the region of the ρ bands with a uniform distribution in the Dalitz plot and with an exponential time decay, with characteristic time equal $0.36\tau_B$. Some results are shown in Figs. 15.

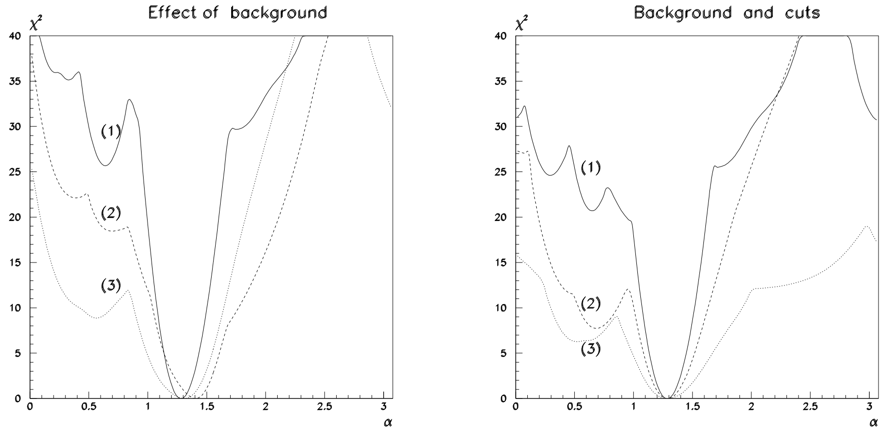

Figure 15: Left hand side: effect of the background. Right hand side: combined effect of background and cuts. In the two cases, the curve number (1) is the reference, the number (2) shows the effect for $B/S = 1$ and the number (3) corresponds to $B/S = 2$. In all cases, there are 600 signal events and the optimistic cuts are used. *The* $\rho(770)$, $\rho(1450)$, *and* $\rho(1700)$ *have all been included.*

Figure 15 shows χ^2 as a function of α $B/S = 1$ (curves (2)) and $B/S = 2$ (curves (3)), with 600 signal events in all cases. On the left hand side only the impact of background is shown, while the right hand side illustrates the combination of background and "optimistic" cuts.

N_{events}	small width (μm)	large width (μm)	fraction correct	$\langle\alpha\rangle \pm \sigma$
600	10	20	0.86	1.367 ± 0.092
600	100	200	0.75	1.366 ± 0.133
600	500	1000	0.74	1.411 ± 0.262

Table 13: Monte Carlo comparison of results for experiments with continuum background. The distribution of the separation of the supposed vertices is the sum of two Gaussians. Of the continuum background, 80% has a smaller width and 20% a larger width. The total number of background events, over the entire Dalitz plot was six times the number of signal events. The results come from 100 simulated experiments. The fraction of the time that the true solution for α was found rather than $\pi/2-\alpha$ is shown as 'fraction correct.' The mean value $\langle\alpha\rangle$ and its σ were computed excluding cases where the mirror solution was preferred.

The left hand figure displays the deterioration in χ^2 as the background increases: the resolution of the smallest minimum gets worse, and the distinction between the two deepest minima is reduced.

When the cuts are added, the situation worsens, but not substantially. This suggests that fighting backgrounds is particularly important, even when cuts are made.

Studying backgrounds across the Dalitz plot

If backgrounds vary only gradually across the Dality plot, there is some advantage to fitting the full background rather than cutting to isolate the ρ. Because the continuum events typically have two jets, it is likely that one combination of two pions will have a relatively small invariant mass, consistent with the ρ. Of course there is no reason for these states to have the $\cos^2\theta$ dependence required of $\rho\pi$ states. *In the simulation,* the preference for two pions to have a small invariant mass was conferred by assigning a matrix element squared proportional to

$$\frac{1}{m^2+\Gamma_{cont}^2/4} \tag{39}$$

where $\Gamma_{cont} = 1$ GeV was chosen, and where m is the smallest of the three di-pion invariant masses. The continuum background will have a different time dependence than the true signal. Most of the events will not have separated vertices, though charm events will, to some extent. The time dependence of the continuum background events was taken to be the sum of two Gaussians, 80% in a narrower Gaussian and 20% in a broader Gaussian. Results for three choices of the widths are given in Table 13. It is apparent from the Table that discriminating against background using vertex separation will be critical and that there will be a premium on vertex resolution.

6.6 Non-resonant background

The non-resonant $B \to 3\pi$ background has the same sort of time structure as the signal, so it is particularly hard to exclude. It is better thought of as the non-resonant part of the signal rather than as a part of the background. We have modeled this with a distribution uniform across the Dalitz plot and with time dependence given just by the B lifetime. As seen in Table 14,

N_{events}	fraction correct	$\langle\alpha\rangle \pm \sigma$
600	0.68	1.389 ± 0.152
1200	0.86	1.356 ± 0.120

Table 14: Monte Carlo comparison of results for experiments with non-resonant $B \to 3\pi$ background. The total number of background events, over the entire Dalitz plot was six times the number of signal events, N_{events}. The mean value $\langle\alpha\rangle$ and its σ were computed excluding cases where the mirror solution was preferred. Without background, 1.369 ± 0.088. See Table 5.5.

increasing the total number of events, while keeping B/S fixed, improves the result. Assuming the distribution is uniform and then fitting its overall strength may underestimate the difficulty of extracting this background.

6.7 Neglecting the $\rho^0\pi^0$ band

The $\rho^0\pi^0$ channel is expected to be color-suppressed (cf. Appendix B). Moreover, this will be compounded by the difficulty *posed by* merged photons coming from higher energy π^0s. If the background in this channel overwhelms the signal, it may be appropriate simply to cut out the $\rho^0\pi^0$ band. A simulation of a 600-event experiment is shown in Figure 16. There is a substantial

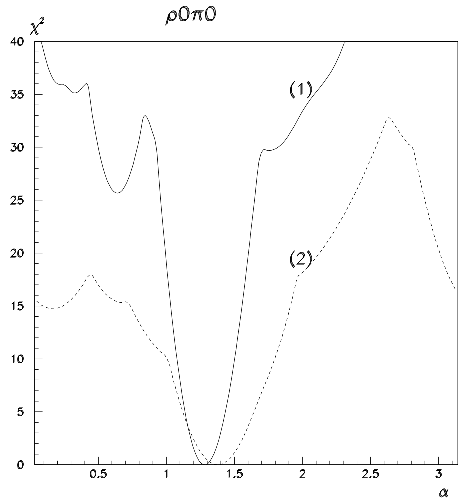

Figure 16: Effect of a cut on the $\rho^0\pi^0$ band: the function number (1) illustrates the perfect case while the number (2) shows the χ^2 for an analysis for which the $\rho^0\pi^0$ events have been removed.

loss in discrimination against the mirror solution when the $\rho^0\pi^0$ band is deleted. The substantial difference between χ^2 at the true and mirror solutions, both with and without $\rho^0\pi^0$, here is likely an artefact of including the $\rho(1450)$ and $\rho(1700)$ with a priori known phases, as discussed in Section 5.1.

6.8 Impact of the $K\pi\pi$ background

Without an effective particle identification system, the observation of the three pion final state might be obscured by the final state $K\pi\pi$ to judge from the *the predominance of $B \to K\pi$ over $B \to \pi\pi$*. Even with excellent particle identification, there will be some background created by $K\pi\pi$. The expected number of $K\pi\pi$ events with 30 fb^{-1} is of the order of 10 after selection, reconstruction, particle identification and tagging at BaBar [4]. *Since this is not certain, we consider two possibilities : one for which the $K\pi\pi$ events represents 5% of the 600 $\pi\pi\pi$ events in the event sample, and the other for which they represent 20%.*

On the left hand side of Fig. 17 shows χ^2 for three different experiments I don't understand. Three experiments? *of 600 $\pi\pi\pi$ events on top of which is added a contamination of 5% of $K\pi\pi$ events.* The minimum of χ^2 is not shifted and we can conclude that the $K\pi\pi$ background will not be a limiting factor in the case we have 5% $K\pi\pi$ in the 3π selection.

The right hand side of Fig. 17 shows χ^2 for 2000 and for 6000 $\pi\pi\pi$ events with a contamination of 20% $K\pi\pi$. It is evident that here there is a dramatic shift in the location of the minimum of χ^2. Should the level of contamination be this high, a detailed study of $K\pi\pi$ itself would be required.

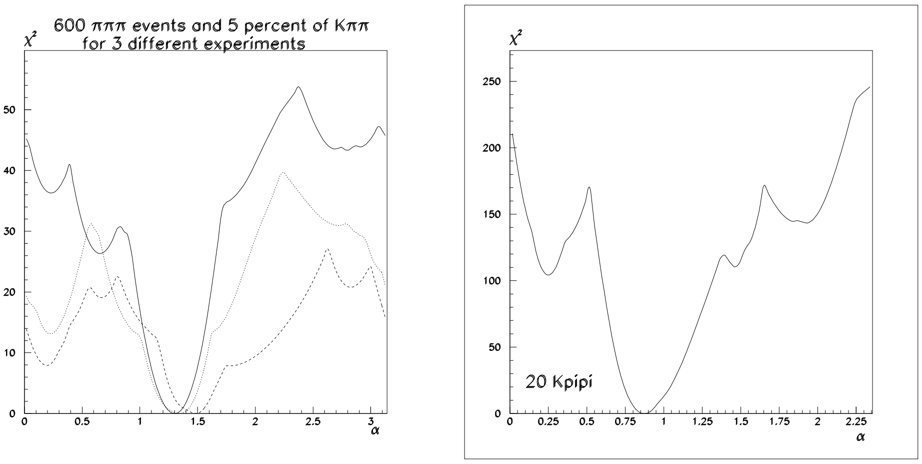

Figure 17: χ^2 *as a function of α Left hand side: for 600 events, with 5% of $K\pi\pi$ events in the sample of $\pi\pi\pi$ events. Three different experiments, differing only in the rnadom choice of events are shown. Right hand side: A Monte Carlo experiment with 6000 events and 20% contamination by $K\pi\pi$.*

7 Recovering information...

7.1 Adding the charged B

If decays to $\pi^0\pi^0\pi^\pm$ can be reconstructed, they charged B decays will provide additional information. In Fig. 18 we show χ^2 without background or detector effects. *The parabola near the absolute minimum is not affected by the addition of these events. Nevertheless, they help discriminate between this minimum and the other ones. It appears that the charged B would provide only modest help in the α determination.*

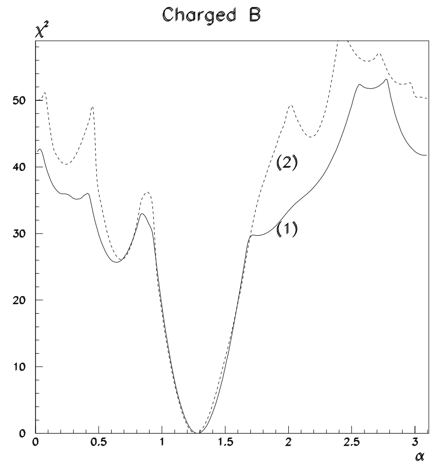

Figure 18: χ^2 for the reference scenario (in plain line) and in the case one adds in the analysis the charged B decays (in dotted line).

7.2 Summary

Need to write this! Probably much like the summary of results near the beginning of the paper.

A Mixing Formalism and Notation

For completeness we review some of the standard defintions and notation used in describing CP violation in the neutral B system. Because second-order weak (and possibly other yet-to-be-discovered) interactions can transform a B^0 into a $\overline{B}^0$ or the reverse, the time development of the $B^0, \overline{B}^0$ system is described by a non-diagonal complex mass matrix

$$i\frac{d}{dt}\begin{pmatrix} a \\ \overline{a} \end{pmatrix} = M \begin{pmatrix} a \\ \overline{a} \end{pmatrix} \tag{40}$$

where

$$M = \begin{pmatrix} M_{11} - i\Gamma_{11}/2 & M_{12} - i\Gamma_{12}/2 \\ M_{21} - i\Gamma_{21}/2 & M_{22} - i\Gamma_{22}/2 \end{pmatrix} \tag{41}$$

From CPT invariance $M_{11} = M_{22}$, $\Gamma_{11} = \Gamma_{22}$, and $M_{21} = M_{12}^*$, $\Gamma_{21} = \Gamma_{12}^*$. The off-diagonal Γ elements give rise to a difference in lifetimes for the two mass eigenstates. This is a small effect compared to the average lifetime for B_d, and we shall ignore it, setting $\overline{M} = M_{11} = M_{22}$, $\Gamma = \Gamma_{11} = \Gamma_{22}$. Diagonalizing the mass matrix we find the complex eigenvalues

$$\begin{aligned} \mu_H &= \overline{M} + |M_{12}| - i\Gamma/2 \equiv \overline{\mu} + \Delta m/2 \\ \mu_L &= \overline{M} - |M_{12}| - i\Gamma/2 \equiv \overline{\mu} - \Delta m/2 \end{aligned} \tag{42}$$

and the corresponding eigenstates

$$\begin{aligned} |B_H\rangle &= \frac{1}{\sqrt{2}}\left(|B^0\rangle + \frac{|M_{12}|}{M_{12}}|\overline{B}^0\rangle\right) \\ |B_L\rangle &= \frac{1}{\sqrt{2}}\left(|B^0\rangle - \frac{|M_{12}|}{M_{12}}|\overline{B}^0\rangle\right) \end{aligned} \tag{43}$$

The time development of states that are pure at $t = 0$ is

$$\begin{aligned} |B^0_{phys}(t)\rangle &= e^{-i\overline{\mu}t}\left[\cos\frac{\Delta m}{2}t\ |B^0\rangle + i(q/p)\sin\frac{\Delta m}{2}t\ |\overline{B}^0\rangle\right] \\ |\overline{B}^0_{phys}(t)\rangle &= e^{-i\overline{\mu}t}\left[\cos\frac{\Delta m}{2}t\ |\overline{B}^0\rangle + i(p/q)\sin\frac{\Delta m}{2}t\ |B^0\rangle\right] \end{aligned} \tag{44}$$

where we used the standard notation

$$q/p = -\frac{|M_{12}|}{M_{12}} = -\frac{|\langle B^0|M|\overline{B}^0\rangle|}{\langle B^0|M|\overline{B}^0\rangle} \tag{45}$$

The decay amplitudes to a final state f are thus

$$\begin{aligned} \langle f|B^0_{phys}(t)\rangle &= e^{-i\overline{\mu}t}\left[\cos\frac{\Delta m}{2}t\ \langle f|\mathcal{H}|B^0\rangle + i(q/p)\sin\frac{\Delta m}{2}t\ \langle f|\mathcal{H}|\overline{B}^0\rangle\right] \\ \langle f|\overline{B}^0_{phys}(t)\rangle &= e^{-i\overline{\mu}t}\left[\cos\frac{\Delta m}{2}t\ \langle f|\mathcal{H}|\overline{B}^0\rangle + i(p/q)\sin\frac{\Delta m}{2}t\ \langle f|\mathcal{H}|B^0\rangle\right] \end{aligned} \tag{46}$$

If the decays were all CP conserving we would have

$$\begin{aligned}\langle f|\mathcal{H}|\overline{B}^0\rangle &= \langle\overline{f}|\mathcal{H}|B^0\rangle/\langle\overline{B}^0|CP|B^0\rangle \\ \langle f|\mathcal{H}|B^0\rangle &= \langle\overline{f}|\mathcal{H}|\overline{B}^0\rangle\langle\overline{B}^0|CP|B^0\rangle\end{aligned} \tag{47}$$

where $CP|f\rangle = |\overline{f}\rangle$. The phase $\langle\overline{B}^0|CP|B^0\rangle$ is a matter of convention and disappears from physical quantities. When there is CP violation, the Hamitonian is a sum of pieces, each with a CP-violating weak phase

$$\mathcal{H} = \sum_j e^{i\phi_j}\mathcal{H}_j + \sum_j e^{-i\phi_j}\mathcal{H}_j^\dagger \tag{48}$$

where $CP\mathcal{H}_iCP = \mathcal{H}_i^\dagger$, so $CP\mathcal{H}CP \neq \mathcal{H}$.

The weak phases of the various contributions come from the CKM matrix. The relations between the CKM matrix elements and the angles of the unitarity triangle are

$$\begin{aligned}\gamma &= arg[-\frac{V_{ud}V_{ub}^*}{V_{cd}V_{cb}^*}] \\ \beta &= arg[-\frac{V_{td}^*V_{tb}}{V_{cd}^*V_{cb}}] \\ \alpha &= arg[-\frac{V_{td}V_{tb}^*}{V_{ud}V_{ub}^*}]\end{aligned} \tag{49}$$

The amplitude for the quark level transition $b \to u\overline{u}d$ has a factor $V_{ub}V_{ud}^*$ while that for the penguin $b \to tW^-$, $tW^- \to dg$ has a factor $V_{tb}V_{td}^*$. The $B^0 - \overline{B}^0$ mixing is dominated by t quark intermediates, with the result

$$(q/p) = \frac{V_{tb}^*V_{td}}{V_{tb}V_{td}^*}\langle\overline{B}^0|CP|B^0\rangle = e^{-2i\beta}\frac{V_{cd}V_{cb}^*}{V_{cd}^*V_{cb}}\langle\overline{B}^0|CP|B^0\rangle \tag{50}$$

This form displays the dependence of (q/p) on the choice of phases for B^0 and $\overline{B}^0$. This dependence just compensates the convention dependence in the rest of the expressions for $\langle f|B^0_{phys}(t)\rangle$ and $\langle f|\overline{B}^0_{phys}(t)\rangle$ so that the expressions for the rates indeed have no convention dependence.

We can harmlessly divide all the amplitudes by $-V_{cd}V_{cb}^*$ and write tree and penguin contributions for both the B^0 and $\overline{B}^0$ decays *to* $u\overline{u}d\overline{d}$ *final states*:

$$\begin{aligned}-\frac{\langle f|\mathcal{H}|B^0\rangle}{V_{cd}V_{cb}^*} &= -e^{i\gamma}T + e^{-i\beta}P \\ -\frac{\langle\overline{f}|\mathcal{H}|\overline{B}^0\rangle}{V_{cd}V_{cb}^*}(q/p) &= e^{-2i\beta}[-e^{-i\gamma}T + e^{i\beta}P]\end{aligned} \tag{51}$$

Again, with impunity we can multiply both amplitudes by $e^{i\beta}$. Using $\alpha+\beta+\gamma=\pi$, we drop an overall constant to write

$$\begin{aligned}\langle f|\mathcal{H}|B^0\rangle &= e^{-i\alpha}T + P \\ \langle\overline{f}|\mathcal{H}|\overline{B}^0\rangle(q/p) &= e^{i\alpha}T + P\end{aligned} \tag{52}$$

In the absence of CP violation, the amplitudes for $B^0 \to \rho^+\pi$ and $\overline{B}^0 \to \rho^-\pi^+$ would be the same. CP violation breaks this relation through the introduction of non-trivial phases. We can display the amplitudes for all the $\rho\pi$ final states as

$$\begin{array}{lclclcll}
A(B^0 \to \rho^+\pi^-) & \equiv & A^{+-} & = & e^{-i\alpha}T^{+-} & + & P^{+-} & , \\
A(B^0 \to \rho^-\pi^+) & \equiv & A^{-+} & = & e^{-i\alpha}T^{-+} & + & P^{-+} & , \\
A(B^0 \to \rho^0\pi^0) & \equiv & A^{00} & = & e^{-i\alpha}T^{00} & + & P^{00} & , \\
A(\overline{B^0} \to \rho^+\pi^-) & \equiv & \overline{A}^{+-} & = & e^{+i\alpha}T^{-+} & + & P^{-+} & , \\
A(\overline{B^0} \to \rho^-\pi^+) & \equiv & \overline{A}^{-+} & = & e^{+i\alpha}T^{+-} & + & P^{+-} & , \\
A(\overline{B^0} \to \rho^0\pi^0) & \equiv & \overline{A}^{00} & = & e^{+i\alpha}T^{00} & + & P^{00} & .
\end{array} \tag{53}$$

For the decay of $\overline{B}^0_{phys}$ we have absorbed the common factor (p/q).

A.1 Number of Independent Amplitudes

These expressions treat the ρ as a stable particle. There are ostensibly 12 real quantities in the six complex amplitudes $A^{ij}, \overline{A}^{ij}$. Introducing α seems to have overparameterized, since it adds a thirteenth. However, the penguin process is pure $\Delta I = 1/2$ and thus can yield only $I = 0$ and $I = 1$ final states. Thus there are but two penguin amplitudes and in fact

$$P^{00} = -\tfrac{1}{2}(P^{+-} + P^{-+}) \tag{54}$$

As a consequence, there are just 11 independent real numbers to determine, while there are twelve measureable quantities. In fact one common phase is unobservable and if the total rate is ignored the absolute normalization is free. In the end there are 10 observables and 9 free parameters.

A.2 Form of the Breit-Wigner Resonance

Since the ρ is observed as $\pi\pi$, the full amplitude must include the appropriate Breit-Wigner expression. There is, as well, the non-trivial angular dependence from the decay of the spin-one ρ. This introduces a factor $\cos\theta$, where θ is the angle between the line of flight of the ρ and one of its decay pions, in the ρ rest frame. The question of which pion to choose is settled by isospin invariance. The isospin-invariant coupling of ρ to $\pi\pi$ dictates that if the π^+ is chosen for the ρ^+, then the π^+ must be chosen for the ρ^0 and the π^0 for the ρ^-.

In the rest frame of the ρ^+ the energies and momenta of the pions are $E^*_+, E^*_-, E^*_0, p^*_+, p^*_-, p^*_0$ where

$$\begin{aligned}
E^*_+ &= E^*_0 = \tfrac{1}{2}\sqrt{s^+} \\
E^*_- &= \frac{m_B^2 - s^+ - m_\pi^2}{2\sqrt{s^+}}
\end{aligned} \tag{55}$$

Here $s^+ = (p_+ + p_0)^2$, $s^- = (p_- + p_0)^2$, $s^0 = (p_+ + p_-)^2$ are the invariant dipion masses squared. The cosine of the angle between π^+ and the line-of-flight of the ρ^+ is

$$\cos\theta_+ = \frac{E^*_0 E^*_- + m_\pi^2 - s^-/2}{p^*_0 p^*_-} \tag{56}$$

For the ρ^0 we take

$$\cos\theta_0 = \frac{E_0^* E_-^* + m_\pi^2 - s^-/2}{p_0^* p_-^*} \tag{57}$$

while for the ρ^- we use

$$\cos\theta_- = \frac{E_+^* E_-^* + m_\pi^2 - s^0/2}{p_+^* p_-^*} \tag{58}$$

We take for the resonant behavior [19]

$$f(s) \propto \frac{1}{s - m_\rho^2 + i\Pi(s)} \tag{59}$$

where

$$\Pi(s) = \frac{m_\rho^2}{\sqrt{s}} \left(\frac{p}{p_0}\right)^3 \Gamma_\rho(m_\rho^2) \tag{60}$$

where $p = p(s) = \frac{1}{2}\sqrt{s - 4m_\pi^2}$ is the momentum of the daughter pion in the ρ rest frame and $p_0 = p(m_\rho^2)$. The full amplitude describing the decay of the ρ is the product of $f(s)$ with the appropriate factor of $\cos\theta$.

We combine these factors to make effective amplitudes for the decays of B^0 and $\overline{B}^0$

$$\begin{aligned} \mathcal{A} &= \cos\theta_+ f(s^+)[e^{-i\alpha}T^{+-} + P^{+-}] + \cos\theta_- f(s^-)[e^{-i\alpha}T^{-+} + P^{-+}] + \cos\theta_0 f(s^0)[e^{-i\alpha}T^{00} + P^{00}] \\ \overline{\mathcal{A}} &= \cos\theta_+ f(s^+)[e^{i\alpha}T^{+-} + P^{+-}] + \cos\theta_- f(s^-)[e^{i\alpha}T^{-+} + P^{-+}] + \cos\theta_0 f(s^0)[e^{i\alpha}T^{00} + P^{00}] \end{aligned} \tag{61}$$

In terms of these, the decay amplitude for a state that is B^0 at $t = 0$ at a later time t is

$$\langle \pi^+\pi^-\pi^0|\mathcal{H}|B^0_{phys}(t)\rangle = exp(-\overline{\mu}t)[\cos\tfrac{1}{2}\Delta mt\mathcal{A} + i\sin\tfrac{1}{2}\Delta mt\overline{\mathcal{A}}] \tag{62}$$

Similarly we have

$$\langle \pi^+\pi^-\pi^0|\mathcal{H}|\overline{B}^0_{phys}(t)\rangle = exp(-\overline{\mu}t)[\cos\tfrac{1}{2}\Delta mt\overline{\mathcal{A}} + i\sin\tfrac{1}{2}\Delta mt\mathcal{A}] \tag{63}$$

In an e^+e^- collider operating at the $\Upsilon(4S)$ the $B^0 - \overline{B}^0$ pairs are produced purely in a p-wave with correlations in their oscillations. One of the neutral B's is tagged to determine whether it is a B^0 or $\overline{B}^0$ and the other is observed in the state of interest. Thus the $B \to \rho\pi$ may be observed before the tag. If a $\overline{B}^0$ is tagged at $t > 0$ after the observed decay to $\rho\pi$ we have

$$\langle \pi^+\pi^-\pi^0|\mathcal{H}|B^0_{phys}(t)\rangle = exp(-\overline{\mu}t)[\cos\tfrac{1}{2}\Delta mt\mathcal{A} - i\sin\tfrac{1}{2}\Delta mt\overline{\mathcal{A}}] \tag{64}$$

while if it is a B^0 that is seen at a time $t > 0$ after the decay

$$\langle \pi^+\pi^-\pi^0|\mathcal{H}|\overline{B}^0_{phys}(t)\rangle = exp(-\overline{\mu}t)[\cos\tfrac{1}{2}\Delta mt\overline{\mathcal{A}} - i\sin\tfrac{1}{2}\Delta mt\mathcal{A}] \tag{65}$$

A.3 If the mixing is non-standard

The Standard Model predicts the mixing phase to be $e^{-2i\beta}$. This could fail if there are important non-Standard Model contributions to the $B^0-\overline{B}^0$ process. If the mixing phase is instead $e^{-2i\tilde{\beta}}$ the analysis can determine $\gamma+\tilde{\beta}$ but not $\gamma+\beta=\pi-\alpha$. Explicitly, consider

$$\begin{aligned} e^{i\tilde{\beta}}A &= -e^{i(\gamma+\tilde{\beta})}T+e^{i(\tilde{\beta}-\beta)}P \\ e^{i\tilde{\beta}}e^{-2i\tilde{\beta}}\overline{A} &= -e^{-i(\gamma+\tilde{\beta})}T+e^{-i(\tilde{\beta}-\beta)}P \end{aligned} \tag{66}$$

which reduce to the usual expressions if $\tilde{\beta}=\beta$. It is possible to determine $\gamma+\tilde{\beta}$ by fitting A^{+-}, A^{-+}, etc. and using

$$\frac{A^{+-}+A^{-+}+2A^{00}}{\overline{A}^{+-}+\overline{A}^{-+}+2\overline{A}^{00}}=e^{2i(\gamma+\tilde{\beta})} \tag{67}$$

On the other hand, if we write generally

$$\begin{aligned} A &= e^{i\phi_T}T+e^{i\phi_P}P \\ \overline{A} &= e^{-i\phi_T}T+e^{-i\phi_P}P \end{aligned} \tag{68}$$

and ask what happens if we try to re-express this as

$$\begin{aligned} A &= e^{i\phi'_T}T'+e^{i\phi'_P}P' \\ \overline{A} &= e^{-i\phi'_T}T'+e^{-i\phi'_P}P' \end{aligned} \tag{69}$$

we find that

$$\begin{aligned} T' &= \frac{\sin(\phi_T-\phi_{P'})T+\sin(\phi_P-\phi_{P'})P}{\sin(\phi_{T'}-\phi_{P'})} \\ P' &= \frac{\sin(\phi_T-\phi_{T'})T+\sin(\phi_P-\phi_{T'})P}{\sin(\phi_{T'}-\phi_{P'})} \end{aligned} \tag{70}$$

In particular, this means that if we assign the wrong phase to the penguin amplitudes, they will no longer satisfy the isospin relation, Eq. (2). That is, if we write generically

$$A=e^{-i\alpha}T+P \tag{71}$$

assuming $\tilde{\beta}=\beta$ when in fact $\tilde{\beta}\neq\beta$, we will get the wrong answer.

In parameterizing the amplitudes we need to impose the isospin constraint without assuming that mixing is given by the Standard Model. A straightforward, if inelegant, way to do this is to take as the independent amplitudes $A^{+-}, A^{-+}, \overline{A}^{+-}, \overline{A}^{-+}, \overline{A}^{00}$ and the single real variable $\phi\equiv\gamma+\tilde{\beta}$. Then in the final amplitude is given in terms of the other variables as

$$A^{00}=e^{-2i\phi}[\tfrac{1}{2}\overline{A}^{+-}+\tfrac{1}{2}\overline{A}^{-+}+\overline{A}^{00}]-\tfrac{1}{2}A^{+-}-\tfrac{1}{2}A^{-+}. \tag{72}$$

We see that we can determine the phase $\tilde{\beta}+\gamma$. What about the phase $\tilde{\beta}-\beta$? Consider the special case of the transformation of Eqs.(68)-(70)with $T'=T$. Then

$$\sin(\phi_T-\phi_{P'})P'=\sin(\phi_T-\phi_P)P \tag{73}$$

In particular, the P' amplitudes will satisfy the isospin constraint. Changing ϕ_P to $\phi_{P'}$ can be achieved simply by shuffling some of P into T, keeping $\sin(\phi_T-\phi_P)P$ fixed. This means that it is in principle impossible to find ϕ_P. By contrast, if we change ϕ_T, with ϕ_P fixed, P will pick up a piece of T, ruining the isospin relation. As long as the isospin relation is obeyed, the phase of the trees is fixed to be $\gamma+\tilde{\beta}$.

B Calculation of the inputs to the Monte Carlo generator

Factorization of the Non-Leptonic Amplitudes

Here we give explicit expressions for the $B \to \rho\pi$ amplitudes in the factorization approximation. The result depends on the Fermi constant G_F, the CKM matrix elements, the decay constants f_π and f_ρ, the $B \to \pi(\rho)$ form factors $f_0(q^2)$ **NOT DEFINED** and $A_0(q^2)$, various masses and kinematical quantities and the following combinations of the short-distance Wilson coefficients c_i $(i = 1 \dots 10)$ [15, 16]

$$a_{2i-1} = c_{2i-1} + \frac{c_{2i}}{3}, \qquad a_{2i} = c_{2i} + \frac{c_{2i-1}}{3} \quad (i = 1 \dots 5). \tag{74}$$

With the notation of Eqs. (4) and (53), and in the limit of exact isospin symmetry of the strong interactions $m_u = m_d \equiv \overline{m}_q$ one has

$$\begin{aligned}
A^{+-} &= F_{\pi\rho}\left[V_{ud}V_{ub}^* a_1 - V_{td}V_{tb}^*(a_4 + a_{10})\right], && (75)\\
A^{-+} &= F_{\rho\pi}\left[V_{ud}V_{ub}^* a_1 - V_{td}V_{tb}^*\left(a_4 + a_{10} - \chi_\pi(a_6 + a_8)\right)\right], && (76)\\
2\,A^{00} &= F_{\pi\rho}\left[V_{ud}V_{ub}^* a_2 - V_{td}V_{tb}^*\left(-a_4 - \frac{3}{2}a_7 + \frac{3}{2}a_9 + \frac{a_{10}}{2}\right)\right] && (77)\\
&+ F_{\rho\pi}\left[V_{ud}V_{ub}^* a_2 - V_{td}V_{tb}^*\left(-a_4 - \frac{3}{2}a_7 + \frac{3}{2}a_9 + \frac{a_{10}}{2} + \chi_\pi(a_6 - \frac{a_8}{2})\right)\right], && (78)\\
\sqrt{2}\,A^{+0} &= F_{\pi\rho}\left[V_{ud}V_{ub}^* a_1 - V_{td}V_{tb}^*(a_4 + a_{10})\right] && (79)\\
&+ F_{\rho\pi}\left[V_{ud}V_{ub}^* a_2 - V_{td}V_{tb}^*\left(-a_4 - \frac{3}{2}a_7 + \frac{3}{2}a_9 + \frac{a_{10}}{2} + \chi_\pi(a_6 - \frac{a_8}{2})\right)\right], && (80)\\
\sqrt{2}\,A^{0+} &= F_{\pi\rho}\left[V_{ud}V_{ub}^* a_2 - V_{td}V_{tb}^*\left(-a_4 - \frac{3}{2}a_7 + \frac{3}{2}a_9 + \frac{a_{10}}{2}\right)\right] && (81)\\
&+ F_{\rho\pi}\left[V_{ud}V_{ub}^* a_1 - V_{td}V_{tb}^*\left(a_4 + a_{10} - \chi_\pi(a_6 + a_8)\right)\right]. && (82)
\end{aligned}$$

In the expressions above we have used the shorthands

$$\begin{aligned}
F_{\pi\rho} &= \frac{G_F}{\sqrt{2}}\, 2m_B p\, f_\rho\, f_+(m_\rho^2), && (83)\\
F_{\rho\pi} &= \frac{G_F}{\sqrt{2}}\, 2m_B p\, f_\pi\, A_0(m_\pi^2), && (84)\\
\chi_\pi &= \frac{m_\pi^2}{\overline{m}_q(m_b + \overline{m}_q)}. && (85)
\end{aligned}$$

SHOULD WE QUOTE $B \to f_0(f_2)\pi^0$? *NO. AND WE DIDN'T DEFINE* m_q. *SHOULD WE LIST THE VALUES OF THE a's?*

Note that in the factorization approximation, the color-suppression of the $\rho^0\pi^0$ channel with respect to the others is due to the ratio $a_2/a_1 \sim 0.2$. The terms proportional to $a_{1,2}$ correspond to the tree diagrams, those proportional to $a_{3,\dots,6}$ to gluonic penguins, and those proportional to $a_{7,\dots,10}$ to electroweak penguins. The numerical value of the Wilson coefficients has been taken in the NDR *NOT DEFINED* renormalization scheme at a scale $\mu \sim m_b$, as reviewed in Ref. [15]. The amplitudes for $B \to K^*\pi$ and $B \to K\rho$ have been calculated similarly. The electroweak penguins terms have been put to zero in the scenarios for the Monte-Carlo generators. It remains to estimate the form factors $f_+(q^2)$ and $A_0(q^2)$, which is the purpose of the next section.

Heavy-to-Light Form Factors

To provide numerical input for the Monte-Carlo generators, we have used the model of Ref. [17]. The form factors were extrapolated from those for $D \to K(K^*)$, the latter being extracted from the experimental data [12], using heavy quark and flavor SU(3) symmetries and a pole model for the q^2 dependence. The result was

$$f_+(q^2) = \frac{0.46}{1 - \frac{q^2}{(m_B+m_\pi)^2}}, \tag{86}$$

$$A_0(q^2) = \frac{0.35}{1 - \frac{q^2}{(m_B+m_\rho)^2}}. \tag{87}$$

As these are evaluated at $q^2 = m_\rho^2$ and $q^2 = m_\pi^2$, respectively, the denominators are nearly unity. Putting the numbers in Eqs. (75)-(87), all together we arrive at the amplitudes and branching ratios of the "Small Penguins" scenario in Tables 4 and 5. We would like to stress that these numbers are only indicative, and that experimental ones may be very different. As can be seen from these tables, the factorization model has definite predictions, the reliability of which is not clear:

1. It incorporates color-suppression of the $\rho^0\pi^0$ channel, because of the ratio $a_2/a_1 \sim 0.2$.
2. It predicts small penguin contributions, particularly in the $B^0 \to \rho^-\pi^+$ channel where contributions of different signs almost cancel each other.
3. It does not take into account any final state interactions effects. As a consequence, there is no non-trivial *CP*-conserving phase in the amplitudes.
4. In addition, the form factors of Eqs. (86) and (87) have a quite high overall normalization compared to other approaches, which in turns imply rather large $B \to \rho\pi$ branching ratios.

The color-suppression of the neutral ρ band handicaps the analyses. By not considering a scenario without color suppression we have made a conservative choice. However, in order to investigate the impact of Points (2) and (3) on the analyses, we have defined another set of parameters ("Large Penguins") with larger penguin to tree ratios, and some arbitrarily chosen strong phases, as well as a zero-penguin scenario ("No Penguins"). *DO WE USE THE NO-PENGUINS?*

C Determination of Electroweak Penguins

We denote by A_2 ($\overline{A}_2$) the amplitudes in the isospin-two channel $B^0 \to \rho\pi(I=2)$ ($\overline{B^0} \to \rho\pi(I=2)$)

$$A_2 \equiv A^{+-} + A^{-+} + 2A^{00} \equiv e^{-i\alpha}\, T_2 + P_{\rm EW} \tag{88}$$
$$\overline{A}_2 \equiv \left[\overline{A}^{+-} + \overline{A}^{-+} + 2\overline{A}^{00}\right] \equiv e^{+i\alpha}\, T_2 + P_{\rm EW}\,, \tag{89}$$

We indicate by $a_{\rm dir}^{(I=2)}$ the direct CP-asymmetry

$$a_{\rm dir}^{(I=2)} \equiv \frac{|A_2|^2 - |\overline{A}_2|^2}{|A_2|^2 + |\overline{A}_2|^2}\,, \tag{90}$$

and by $2\alpha_{\rm eff}^{(I=2)}$ the effective 2α angle

$$2\alpha_{\rm eff}^{(I=2)} \equiv {\rm Arg}\left(\overline{A}_2 A_2^*\right) \tag{91}$$

which reduces to 2α in the limit of vanishing electroweak penguin, one finds, in full analogy with Ref. [7],

$$\cos\left[2\alpha - 2\alpha_{\rm eff}^{(I=2)}\right] = \frac{1}{\sqrt{1-\left[a_{\rm dir}^{(I=2)}\right]^2}}\left[1 - \left(1 - \sqrt{1-\left[a_{\rm dir}^{(I=2)}\right]^2}\,\cos 2\alpha_{\rm eff}^{(I=2)}\right)\left|\frac{P_{\rm EW}}{T_2}\right|^2\right]\,. \tag{92}$$

The full Dalitz plot analysis provides in principle, a 10-parameter fit giving all the amplitudes A^{+-}, etc.. and thus the quantities $a_{\rm dir}^{(I=2)}$ and $2\alpha_{\rm eff}^{(I=2)}$ without discrete ambiguity in the general case. Thus it remains to estimate, for example, the ratio $|P_{\rm EW}/T_2|$ to get 2α from Eq. (92) up to a twofold discrete ambiguity. This estimation has to come from the theory. Alternatively, one may simply plot 2α as a bivalued function of the ratio $|P_{\rm EW}/T_2|$.

Several authors [18] have recently noted that for the two-pion channel there is a very simple relation between the $\Delta I = 3/2$ electroweak penguin amplitude and the corresponding tree one, provided one neglects the contribution of the operators O_7 and O_8. The latter approximation is justified because these operators come with much smaller Wilson coefficients than the two other electroweak penguin operators O_9 and O_{10} [15, 16]. This model-independent determination of the electroweak penguin effects may be applied to $\rho\pi$ as well. Here the $\Delta I = 3/2$ amplitude is the sum $A^{+-} + A^{-+} + 2A^{00}$. Following the calculation of Ref. [18], one is able to determine the ratio $P_{\rm EW}/T_2$ if one neglects the contribution of the operators O_7 and O_8:

$$\frac{P_{\rm EW}}{T_2} \simeq \frac{3}{2}\frac{c_9 + c_{10}}{c_1 + c_2}\left|\frac{V_{td}V_{tb}}{V_{ud}V_{ub}}\right| = -\,(1.31 \pm 0.15) \times 10^{-2} \times \left|\frac{V_{td}V_{tb}}{V_{ud}V_{ub}}\right|\,, \tag{93}$$

where the numerical value of the above ratio of Wilson coefficients and its theoretical uncertainty have been taken from Refs. [15, 16] and considering the residual renormalization scale- and scheme-dependence as well as the neglect of the operators O_7 and O_8 [2]. Then using Eq. (93)

[2] It is assumed that the matrix elements of O_7 and O_8 are not particularly enhanced with respect to those of O_9 and O_{10}, which is indeed the case in an explicit model-dependent calculation based on the factorization assumption (see Section B).

in Eq. (92), and performing a full three-pion Dalitz plot analysis, it is possible to get 2α, taking into account electroweak penguin contributions. To avoid the problem of knowing the ratio $|V_{td}/V_{ub}|$, it is possible to express the latter ratio as well as the angle α in terms of ρ and η, and to solve directly Eq. (92) in the (ρ, η) plane [7]. It would only be a minor refinement, though, because of the tiny numerical value of the ratio (93).

Note that the approximate relation (93) implies that the direct CP-asymmetry in the $I = 2$ channel, $a_{\rm dir}^{(I=2)}$, vanishes: this prediction could be tested experimentally. Finally we would like to stress that while the electroweak penguins are not expected to induce a large shift on α, they may contribute significantly to the $B \to \rho^0 \pi^0$ branching ratio (see our model in Appendix B).

D Parameterization schemes and MINUIT minimization

In order to scan the *nine-parameters space an optimal way*, we have defined a parameterization differing from the one proposed in Ref. [3]. We write the A^{ij} amplitudes as:

$$A^{ij} \;=\; \mid A^{ij} \mid e^{i\Psi^{ij}} \;, \tag{94}$$

and the $\overline{A^{ij}}$ using:

$$\overline{A^{+-}} \;=\; \mid A^{-+} \mid a_1 e^{i(\Psi^{+-}-\phi_1)} \tag{95}$$

$$\overline{A^{-+}} \;=\; \mid A^{+-} \mid a_2 e^{i(\Psi^{-+}-\phi_2)} \tag{96}$$

$$\overline{A^{00}} \;=\; \mid A^{00} \mid a_3 e^{i(\Psi^{00}-\phi_3)} \;. \tag{97}$$

Type of interference	Amplitudes	Breit Wigners	Parameterization eq.(94)-(95) Amplitudes	Phases
I_0	$A^{+-*}A^{+-}$	$\mid f^{+} \mid^2$	$\mid A^{+-} \mid^2$	None
I_0	$A^{-+*}A^{-+}$	$\mid f^{-} \mid^2$	$\mid A^{-+} \mid^2$	None
I_0	$A^{00*}A^{00}$	$\mid f^{0} \mid^2$	$\mid A^{00} \mid^2$	None
I_0	$\overline{A^{+-}}^*\overline{A^{+-}}$	$\mid f^{+} \mid^2$	$\mid A^{-+} \mid^2 a_1$	None
I_0	$\overline{A^{-+}}^*\overline{A^{-+}}$	$\mid f^{-} \mid^2$	$\mid A^{+-} \mid^2 a_2$	None
I_0	$\overline{A^{00}}^*\overline{A^{00}}$	$\mid f^{0} \mid^2$	$\mid A^{00} \mid^2 a_3$	None
I_1	$A^{+-*}A^{-+}$	$f^{+*}f^{-}$	$\mid A^{+-} \mid\mid A^{-+} \mid$	$\Psi^{-+} - \Psi^{+-}$
I_1	$A^{+-*}A^{00}$	$f^{+*}f^{0}$	$\mid A^{+-} \mid\mid A^{00} \mid$	$\Psi^{00} - \Psi^{+-}$
I_1	$A^{-+*}A^{00}$	$f^{-*}f^{0}$	$\mid A^{-+} \mid\mid A^{00} \mid$	$\Psi^{00} - \Psi^{-+}$
I_1	$\overline{A^{+-}}^*\overline{A^{-+}}$	$f^{+*}f^{-}$	$\mid A^{-+} \mid\mid A^{+-} \mid a_1 a_2$	$\Psi^{-+} - \Psi^{+-} + \phi_1 - \phi_2$
I_1	$\overline{A^{+-}}^*\overline{A^{00}}$	$f^{+*}f^{0}$	$\mid A^{-+} \mid\mid A^{00} \mid a_1 a_3$	$\Psi^{00} - \Psi^{+-} + \phi_1 - \phi_3$
I_1	$\overline{A^{-+}}^*\overline{A^{00}}$	$f^{-*}f^{0}$	$\mid A^{+-} \mid\mid A^{00} \mid a_2 a_3$	$\Psi^{00} - \Psi^{-+} + \phi_2 - \phi_3$
I_2	$A^{-+*}\overline{A^{-+}}$	$\mid f^{-} \mid^2$	$\mid A^{-+} \mid\mid A^{+-} \mid a_2$	$-\phi_1$
I_2	$A^{+-*}\overline{A^{+-}}$	$\mid f^{+} \mid^2$	$\mid A^{+-} \mid\mid A^{-+} \mid a_1$	$-\phi_2$
I_2	$A^{00*}\overline{A^{00}}$	$\mid f^{0} \mid^2$	$\mid A^{00} \mid\mid A^{00} \mid a_3$	$-\phi_3$
I_3	$A^{+-*}\overline{A^{-+}}$	$f^{+*}f^{-}$	$\mid A^{+-} \mid\mid A^{+-} \mid a_2$	$\Psi^{-+} - \Psi^{+-} - \phi_2$
I_3	$A^{+-*}\overline{A^{00}}$	$f^{+*}f^{0}$	$\mid A^{+-} \mid\mid A^{00} \mid a_3$	$\Psi^{00} - \Psi^{+-} - \phi_3$
I_3	$A^{-+*}\overline{A^{+-}}$	$f^{-*}f^{+}$	$\mid A^{-+} \mid\mid A^{-+} \mid a_1$	$\Psi^{+-} - \Psi^{-+} - \phi_1$
I_3	$A^{-+*}\overline{A^{00}}$	$f^{-*}f^{0}$	$\mid A^{-+} \mid\mid A^{00} \mid a_3$	$\Psi^{00} - \Psi^{-+} - \phi_3$
I_3	$A^{00*}\overline{A^{+-}}$	$f^{0*}f^{+}$	$\mid A^{00} \mid\mid A^{-+} \mid a_1$	$\Psi^{+-} - \Psi^{00} - \phi_1$
I_3	$A^{00*}\overline{A^{-+}}$	$f^{0*}f^{-}$	$\mid A^{00} \mid\mid A^{+-} \mid a_2$	$\Psi^{-+} - \Psi^{00} - \phi_2$

Table 15: Bilinear terms appearing in the decay rates.

All the terms of the likelihood function are summarized in Table 15. They are grouped according to the type of interferences in which they appear (cf. Section 2.4): the I_1 terms appear through cosine in the matrix elements, and the I_2 and I_3 appear through sine.

Approximate Symmetries of the likelihood function

If the interference where bands cross is ignored, dropping categories I_1 and I_3, the contributing terms are invariant under.

$$\phi_1 \rightarrow \pi - \phi_1 \text{ or/and} \tag{98}$$
$$\phi_2 \rightarrow \pi - \phi_2 \text{ or/and} \tag{99}$$
$$\phi_3 \rightarrow \pi - \phi_3 \ . \tag{100}$$

This is true independently of the Penguin contributions. In the case we also neglect these contributions, as well as the $\rho^0\pi^0$ contributions, one may recover the usual mirror solutions of Table 2.

In addition to these transformations that leave invariant the likelihood function except for the interferences between the ρ bands, one may derive another set

$$\Psi^{-+} \rightarrow 2\Psi^{+-} - \Psi^{-+} \text{ and} \tag{101}$$
$$\Psi^{00} \rightarrow 2\Psi^{+-} - \Psi^{00} \tag{102}$$

that leave invariant the I_1 terms if one removes the variation of the phase of the Breit Wigner over the Dalitz Plot.

If one combines all these transformations (from equations (98) to (101)), the complete likelihood function is invariant in the case that ρ is small. This transformation,

$$A^{ij} \rightarrow A^{ij*} \tag{103}$$
$$\overline{A^{ij}} \rightarrow -\overline{A^{ij*}} \tag{104}$$

This corresponds to the well known mirror solution $\alpha \rightarrow \pi/2 - \alpha$ one obtains when the penguins, and the $\rho^0\pi^0$ events are neglected (cf. table 2).

Minimal Parameterization If the penguins contribute only to $\Delta I = 1/2$ (cf. Section 2.1) processes, one may derive a relation between the A^{ij} matrix element in the parameterization described in the previous sections:

$$\overline{A^{00}} = \frac{1}{2}[(A^{+-} + A^{-+} + 2A^{00})e^{2i\alpha} - \overline{A^{+-}} - \overline{A^{-+}}] \quad . \tag{105}$$

This reduces the number of parameters to nine: A^{-+}, Ψ^{-+}, a_1, a_2, a_3, ϕ_1, ϕ_2, ϕ_3, α, where we chose here to fix the values of Ψ^{+-} and A^{+-} since we are not measuring the actual decay rate and since one phase may be fixed arbitrarily.

With this parameterization, the mirror solutions are easily identified. The penguins appear as deviations of the a's from unity. Eq. (105) also makes manifest that it is 2α that enters, not α Replacing α by $\alpha + \pi$ has no physical consequence.

It is possible to fit without imposing Eq. (105). Then the relation

$$\mid \frac{A^{+-} + A^{-+} + 2A^{00}}{\overline{A^{+-}} + \overline{A^{-+}} + 2\overline{A^{00}}} \mid = 1 \tag{106}$$

tests the proposition that the penguins are purely $\Delta I = 1/2$. The failure of the relation would point to a large electroweak penguin contribution.

In practice, the nine-parameter analysis is done by fixing α and varying the remaining eight parameters to maximize the log-likelihood. Once a local maximum is found, relations (98) to (101 are used to search for other maxima, which might be better still. More precisely,

- 1. The initial condition is to set all the phases to zero and all the moduli to 1.1: we choose 1.1 instead of 1 since $a_i = 1$ corresponds to the special configuration for with no penguins.
- 2. We scan the range $[0 : \pi]$ for the α values, and in each point we do a 8 parameters fit.
- 3. Once the above fit has converged, we apply the mirror solutions transformations and ask Minuit to search the vicinity for an improved maximum.
- 4. Finally we go return to item (2) and calculate with the next value of α.

In addition, we also scan in α from π to 0. The need for this is displayed in Sec. 5.1.

Références

[1] R. Aleksan, I. Dunietz, B. Kayser, and F. LeDiberder, *Nucl. Phys.* **B361**, 1414 (1991).

[2] H. J. Lipkin *et al.*, Phys. Rev. **D44**, 1454 (1991).

[3] A. E. Snyder and H. R. Quinn, Phys. Rev. **D48**, 2139 (1993).

[4] *The BaBar Physics Book*, eds. P. F. Harrison and H. R. Quinn, SLAC-R-504 (1998).

[5] S. Versillé: Thesis of Paris XI University, Orsay, *La violation de CP dans BaBar: étiquetage de mésons B et étude du canal* $B \to 3\pi$. 15 Avril 1999.

[6] M. Gronau and D. London, Phys. Rev. Lett. **65**, 3381 (1990)

[7] J. Charles, Phys. Rev. **D59**, 054007 (1999).

[8] Y. Kwon et al., CLEO Collaboration, "Study of charmless hadronic B decays into the final states $K\pi$, $\pi\pi$, and KK, with the first observation of $B \to \pi^+\pi^-$ and $B \to K^0\pi^0$, submitted to the 19th International Symposium on Lepton and Photon Interactions at High Energies, Stanford, CA, 9 - 14 August, 1999.

[9] Y. Gao and F. Würthwein (CLEO Collaboration), CALT-68-2220, hep-ex/9904008 To be published in the Proceedings of American Physical Society Meeting of the Division of Particles and Fields (DPF 99), Los Angeles, CA, 5-9 Jan 1999.

[10] ALEPH Collaboration, R. Barate *et al.*, Z. f. Phys. **C76**,15, (1997).

[11] Particle Data Group (C. Caso *et al.*), Eur. Phys. J. C. **C3**, (1998).

[12] Fermilab REF NEEDS COMPLETION

[13] The BaBar Collaboration,
Technical Design Report 1995

[14] LHC-B collaboration
LHC-B Technical Proposal, CERN/LHCC 98-4.

[15] G. Buchalla, A. J. Buras and M. E. Lautenbacher, Rev. Mod. Phys. **68** 1125 (1996).

[16] M. Ciuchini *et al.*, Z. Phys. **C68** 239 (1995).

[17] R. Aleksan *et al.*, Phys. Lett. **B356**, 95 (1995).

[18] M. Neubert and J. L. Rosner, Phys. Lett. **B441** (1998); Phys. Rev. Lett. **81** 5076 (1998); A. J. Buras and R. Fleischer, hep-ph/9810260; M. Gronau, D. Pirjol and T.-M. Yan, hep-ph/9810482.

[19] J.H.Kühn, and A.Santamaria.
Z.Phys C48(1990) 445.